

**MODELING WATER QUALITY PARAMETERS USING  
LANDSAT 8 AND ASD HYPERSPECTRAL  
SPECTRORADIOMETER DATA: A CASE STUDY OF  
KHANPUR DAM**



*By*

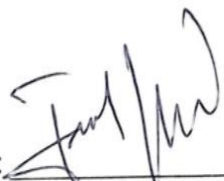
**Syeda Fatima Gillani  
(2021-NUST-MS-363940)**

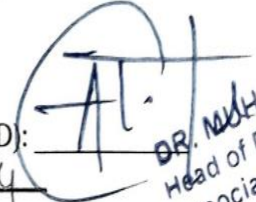
**A thesis submitted in partial fulfillment of the requirements for  
the degree of Master of Science in Remote Sensing and GIS**


**Institute of Geographical Information Systems  
School of Civil and Environmental Engineering  
National University of Sciences and Technology  
Islamabad, Pakistan  
July 2024**

## THESIS ACCEPTANCE CERTIFICATE

Certified that final copy of MS/MPhil thesis written by Syeda Fatima Gillani (Registration No. MSRSGIS 00000363940), of Session 2021 (Institute of Geographical Information Systems) has been vetted by undersigned, found complete in all respects as per NUST Statutes/Regulation, is free of plagiarism, errors, and mistakes and is accepted as partial fulfillment for award of MS/MPhil degree. It is further certified that necessary amendments as pointed out by GEC members of the scholar have also been incorporated in the said thesis.

Signature:   
Name of Supervisor: Dr Javed Iqbal  
Date: 29/7/2024

Signature (HOD):   
Date: 8.8.24  
**DR. MUHAMMAD ALI TAHIR**  
Head of Department  
Associate Professor  
SCEE (IGIS)  
NUST. H-12 Islamabad

Signature (Principal & Dean SCEE):   
Date: 09 AUG 2024

**PROF DR MUHAMMAD IRFAN**  
Principal & Dean  
SCEE, NUST

## DEDICATION

*To*

*My Beloved Mother*

*Thanks for her unwavering support and boundless love, her encouragement and sacrifices have been the pillars of my academic journey. Thank you for being my guiding light throughout this endeavor.*

## ACADEMIC THESIS: DECLARATION OF AUTHORSHIP

I, Syeda Fatima Gillani declare that this thesis and the work presented in it are my own and have been generated by me as the result of my own original research.

**“Modeling water quality parameters using Landsat 8 and ASD Hyperspectral spectroradiometer data: A case study of Khanpur Dam”**

I confirm that:

- This work was done wholly by me in candidature for an MS research degree at the National University of Sciences and Technology, Islamabad.
- Wherever I have consulted the published work of others, it has been clearly attributed.
- Wherever I have quoted from the work of others, the source has always been cited.
- I have acknowledged all main sources of help.
- None of this work has been published before submission. This work is not plagiarized under the HEC plagiarism policy.

Signed: 

Date: 12-08-2024

## **ACKNOWLEDGEMENTS**

### **“In the name of Allah, the most merciful and beneficent”**

All praises to Allah Almighty the most merciful and benevolent, without whose consent nothing would ever be imaginable. Blessings upon Prophet Muhammad (peace be upon Him) for He is a beacon as I pace on in my life and work.

I am profoundly grateful to my respected research supervisor Dr. Javed Iqbal for his unwavering guidance and mentorship throughout the research. I am thankful to Sir Junaid Aziz Khan who helped me out in the collection of spectral signatures and to all the staff that was there to assist. I am indebted to my teachers for their invaluable guidance and constructive feedback.

I extend my heartfelt gratitude to my mother for her undying love and motivation, which has been my driving force. To my sisters, your encouragement made this journey smoother.

A special thanks to my friends especially Sana Zarwania, Misbah Ihsan, and Rida Maqsood for standing by me through thick and thin. Each one of you played a crucial role in shaping my academic path. Together, you all have been the pillars of my success. Thank you for being a part of this significant chapter in my life.

Nevertheless, it is an inspiration that I derived from the unconditional love, support, and prayers of my parents, friends, and family that have propelled me as far as I have triumphed.

**Syeda Fatima Gillani**

## TABLE OF CONTENTS

CERTIFICATE.....	<i>ii</i>
DEDICATION .....	<i>iii</i>
ACADEMIC THESIS: DECLARATION OF AUTHORSHIP .....	<i>iv</i>
ACKNOWLEDGEMENTS.....	<i>v</i>
LIST OF FIGURES .....	<i>vii</i>
LIST OF TABLES .....	<i>viii</i>
TABLE OF ABRIVATIONS.....	<i>ix</i>
ABSTRACT.....	<i>xi</i>
Chapter 1: Introduction.....	<i>1</i>
1.1 Background .....	<i>1</i>
1.2 Significant Water Quality Parameters .....	<i>3</i>
1.3 Laboratory Analysis and Remote Sensing of Water Quality Parameters.....	<i>5</i>
1.4 Spectral Response of Water Bodies .....	<i>7</i>
1.5 Significance of the Study .....	<i>9</i>
1.6 Research Gap .....	<i>12</i>
1.7 Objectives .....	<i>12</i>
Chapter 2: Literature Review.....	<i>13</i>
2.1 Water Quality Modeling in Pakistan .....	<i>13</i>
2.2 Remote Sensing of Water Quality Assessment Across the Globe .....	<i>16</i>
Chapter 3: Material and Methods .....	<i>22</i>
3.1 Study Area.....	<i>22</i>
3.2 Brief Description of Methodology.....	<i>22</i>
3.2.1 Field Water Sampling.....	<i>24</i>
3.2.2 Laboratory Analysis .....	<i>26</i>
3.2.3 ASD-Hyperspectral Spectroradiometer Data Analysis.....	<i>29</i>
3.2.4 Multi-spectral Landsat 8 OLI Data .....	<i>32</i>
3.2.5 Multiple Linear Regression Model .....	<i>32</i>
3.2.6 Model Validation.....	<i>33</i>
Chapter 4: Results and Discussions .....	<i>35</i>
4.1 Results of Laboratory Analysis .....	<i>35</i>
4.2 ASD Spectral Signatures Processing .....	<i>38</i>
4.3 Comparison Between Multispectral and Hyperspectral Data.....	<i>39</i>
4.3.1 Bands Selection.....	<i>39</i>
4.3.2 Regression Model .....	<i>39</i>
4.4 Model Validation.....	<i>45</i>
4.4.1 Turbidity.....	<i>45</i>
4.4.2 Phosphate .....	<i>45</i>
4.4.3 Nitrate .....	<i>48</i>
4.5 Water Quality Indices.....	<i>50</i>
4.5.1 Normalized Difference Chlorophyll Index (NDCI).....	<i>50</i>
4.5.2 Normalized Difference Turbidity Index (NDTI) .....	<i>50</i>
Chapter 5: Conclusions and Recommendations .....	<i>54</i>
5.1 Conclusions.....	<i>54</i>
5.2 Recommendations.....	<i>55</i>
REFERENCES.....	<i>57</i>

## LIST OF FIGURES

Figure 1.1.Spectral response of different elements in clear water body. ....	10
Figure 1.2.Spectral response of Tangxun lake, China.....	10
Figure 1.3.Spectral response of Krishnarajapuram lake, Banglore. ....	11
Figure 1.4.Spectral response of Barra Bonita hydroelectric reservoir. ....	11
Figure 3.1.Study area. ....	23
Figure 3.2.Khanpur dam ariel photograph. (Source: <a href="https://twitter.com/amazing_pk/status/947384075156885504">https://twitter.com/amazing_pk/status/947384075156885504</a> ).....	23
Figure 3.3. Methodology flow chart .....	25
Figure 3.4 Field sampling .....	27
Figure 3.5. Laboratory analysis in IESE lab, NUST.....	30
Figure 3.6. Raw reflectance signatures collected from ASD spectroradiometer. ....	31
Figure 3.7. Post-processed reflectance signatures. ....	31
Figure 4.1. ASD-hyperspectral reflectance signatures from 25 different locations of Khanpur dam.....	40
Figure 4.2 (a) Regression Model of Turbidity and Wavelength ratio 560/891nm ratio of ASD; (b) Regression Model of Turbidity and OLI_Band3/Band4 ratio; (c) Regression Model of Turbidity and ASD Wavelength 600/820nm ratio; (d) Regression Model of Turbidity and OLI_B .....	42
Figure 4.3 a) Regression Model of Phosphate and ASD Wavelength 560/891nm ratio; (b) Regression Model of Phosphate and OLI_Band3/Band5 ratio; (c) Regression Model of Phosphate and ASD Wavelength 600/820nm ratio; (d) Regression Model of Phosphate and OLI_Band4/Band5 .....	43
Figure 4.4 a) Regression Model of Nitrate and ASD Wavelength 465/729nm ratio; (b) Regression Model of Nitrate and OLI_Band2/Band5 ratio; (c) Regression Model of Nitrate and ASD Wavelength 600/820nm ratio; (d) Regression Model of Nitrate and OLI_Band4/Band5 .....	44
Figure 4.5. Normalized difference chlorophyll index map of Khanpur Dam.....	52
Figure 4.6. Normalized difference turbidity index map of Khanpur Dam. ....	53

## LIST OF TABLES

Table 3.1. Dataset characteristics.....	25
Table 3.2. Permissible limits of water quality parameters. ....	30
Table 4.1. Summary statistics of water quality parameters .....	37
Table 4.2. Correlation matrix of water quality parameters .....	37
Table 4.3. Selected wavelengths and their ranges.....	40
Table 4.4. Model validation results of turbidity with ASD ratios.....	46
Table 4.5. Model validation results of turbidity with OLI ratios. ....	46
Table 4.6. Model validation results of phosphate with ASD ratios.....	47
Table 4.7. Model validation results of phosphate with OLI ratios.....	47
Table 4.8. Model validation results of nitrate with ASD ratios.....	49
Table 4.9. Model validation results of nitrate with OLI ratios.....	49



## TABLE OF ABRIVATIONS

ANN	Artificial Neural Network
ASD	Analytical Spectral Device
Chl-a	Chlorophyll a
DN	Digital Number
DT	Dark Target
EC	Electrical Conductivity
EPA	Environmental Protection Agency
ETM	Enhanced Thematic Mapper
FDT	First Derivative Transform
FLAASH	Fast Line-of-sight Atmospheric Analysis of Spectral Hypercubes
GNDVI	Green Normalized Difference Vegetation Index
GIS	Geographic Information System
GPS	Global Positioning System
KPK	Khyber Pakhtunkhwa
LULC	Land Use Land Classification
MAE	Mean Absolute Error
MCI	Maximum Chlorophyll Index
MLR	Multiple Linear Regression
MR	Multiple Regression
MSR	Multiple Stepwise Regression
MODIS	Moderate Resolution Imaging Spectroradiometer
NDTI	Normalized Difference Turbidity Index
NDCI	Normalized Difference Chlorophyll Index
NDVI	Normalized Difference Vegetation Index
NDWI	Normalized Difference Water Index
NTU	Nephelometric Turbidity Units
OLI	Operational Land Imager

RMSE	Root Mean Square Error
S/m	Siemens per meter
SPC	Statistical Process Control
TDS	Total Dissolved Solids
TSS	Total Suspended Solids
PCR	Principal Component Regression
PLSR	Principal Least Square Regression
PCRWR	Pakistan Council of Research In Water Resources
r	Correlation Coefficient
R <sup>2</sup>	Coefficient of Determination
RS	Remote Sensing
SG	Savitzky-Golay
SMLR	Stepwise Multiple Linear Regression
SWIR	Short-wave Infrared
TIRS	Thermal Infrared sensor
UAV	Unmanned aerial Vehicles.
UNEP	United Nations Environment Program
USGS	United States Geological Survey
UV	Ultra-Violet
Vis-NIR	Visible Near Infra-Red Spectroscopy
WHO	World Health Organization
WQI	Water Quality Index

## ABSTRACT

Water contamination in Pakistan is a serious public health concern made worse by the country's growing population. Few studies have been conducted to relate remote sensing data to model the water quality parameters. This study used the multispectral and hyperspectral data to relate and model the water quality parameters. Twenty-five randomly selected surface water quality samples were collected from the Khanpur Dam. The spectral data was collected using Landsat 8 and ASD spectroradiometer. Water quality samples were analyzed in the laboratory, using standard analytical techniques for physico-chemical properties (EC, pH, turbidity, nitrates and phosphates) and the regression analysis were applied for model development. The water quality parameters turbidity and phosphate indicates above permissible limits however parameters pH, EC and nitrates were found to be within permissible limits. The nitrate had a high correlation with turbidity ( $r=0.71$ ) and phosphate ( $r=0.68$ ), similarly turbidity with phosphate indicates significant correlation ( $r=0.81$ ). The results of regression models for water quality prediction reveal compelling insights. ASD ratio 560/891 nm for predicting turbidity, yields coefficient of determination ( $R^2=0.75$ ) and root mean square (RMSE) of 0.68. In comparison, the application of the OLI ratio Band3/Band5 within the green spectral range produces an RMSE of 1.04 and  $R^2=0.41$ . For phosphates prediction, the ASD ratio 600/820 nm resulted in RMSE of 0.09 and an  $R^2$  of 0.69, while the OLI ratio Band4/Band5 within the corresponding spectral range (i.e., red), shows similar performance with an RMSE of 0.09 and  $R^2$  of 0.49. Furthermore, for nitrates prediction, the ASD ratio 465/729 nm yielded  $R^2 = 0.74$  and an RMSE of 0.27, whereas, the OLI ratio Band2/Band5 in blue spectral range produced  $R^2 = 0.45$  and an RMSE of 0.38. In summary, the findings show that for all three water quality criteria, ASD ratios consistently performed better than OLI ratios. These generated models may help in informed decision making in water resource management, emphasizing the relevance of established spectral ratios in shaping effective strategies.

### INTRODUCTION

#### 1.1 Background

A country must have high-quality freshwater water resources, such as ponds, wetlands, dams, and rivers that sustain its citizens' daily routines and economic growth-promoting industries like transportation, farming, manufacturing, and recreational. The ecological systems of reservoirs and water quality have been impacted by industrialization and population growth (Murugan et al., 2016). Intense agricultural practices significantly impact the water quantity and quality of water bodies due to rapid population growth and unpredictable environment. The development of dams is an example of how human activities continue to change and impact hydrological operations, such as the movement of sediments and the consequently changed morphology of rivers (Mazhar et al., 2023). The root cause of water contamination in developing countries like Pakistan is the resource shortage and awareness. The origin or habitat where water is found, human activity including the use of water for diverse reasons, and management actions made to preserve that water resource are three variables that have an impact on the quality of water as a whole. Many physical and chemical parameters govern quality of water. One major problem is that the entire globe is now experiencing is water pollution. Drinking polluted water can be hazardous. Untreated sewage discharges, industrial chemicals spilled into the water, and herbicide leaks from farming areas are all potential sources of water pollution (Akbar et al., 2022).

In Pakistan, water pollution is the main health risks to the community. Drinking water quality is not adequately controlled or observed and is deteriorating daily. Pakistan is classed 80th out of 122 nations in terms of the quality of their drinking water. Hazardous minerals, pesticides, and bacteria are present in drinking water sources across the nation, including groundwater and surface waters. The WHO has developed several drinking water quality

standards that are often broken (Khan et al., 2018). In the past 20 years, Islamabad, the capital of Pakistan, has experienced tremendous urban expansion, which has impacted the number and quality of water bodies. Islamabad is a highly populated urban region that has had a 73% rise of inhabitants over the last 15 years, according to data from the World Bank. With a collective population of 1.3 million, Islamabad and Rawalpindi share a climate and natural resources. Freshwater is becoming scarce due to several human activities that pollute water (Sohail et al., 2023). One of the major reservoirs of fresh water near Islamabad is the Khanpur dam, which has been built on the Haro River in the district of Haripur, on the border between the provinces of Punjab and Khyber Pakhtunkhwa (KPK). The twin towns of Rawalpindi and Islamabad, which are situated downhill, receive drinking water from the dam. It is very important because surface water quality affects aquatic ecosystems and human health. The rushing water of the Haro River, which feeds into the Khanpur Dam, is extremely susceptible to contamination because of its function in removing runoff from farmland and industrial and urban effluent from its large drainage basins (Jadoon et al., 2012). There are several advantageous environmental considerations linked to the dam's construction. They serve as a supply of drinking water and are a crucial component of water management. Because during draughts they hold onto water and help to enhance the water's conditions and minimize flood flows (Dębska et al., 2021). Also, the main purpose of its construction was to supply Rawalpindi and Islamabad's citizens with clean water to drink. But as time went by, tourists started coming from across the nation and overseas for leisure activities. In addition, hotels and restaurants were constructed in the vicinity for the benefit of visitors. This has led to the dumping of sewage and animal remains by those restaurants, and farm residences are steadily depleting the water in the reservoir. This is poisoning the water for human consumption in addition to aquatic life. The main cause of contaminated water was construction in the water reservoir's catchment regions without an appropriate sewage infrastructure. Upstream of the dam, relentless

development is a constant source of water contamination that might significantly harm the consumer's health (Mir, 2022).

## **1.2 Significant Water Quality Parameters**

Increased sediment and nutrient fluxes brought about by human-induced perturbations in watershed areas and intensified land use practices contribute to the eutrophication and deterioration of basin-scale hydrological regimes and water quality. Human-caused nutrient and sediment flows affect human consumption and biodiversity while acting as a pollution stressor (Harrison et al., 2010). Current climate change, anthropological behaviors such as urbanization, farming techniques, and industrialization, as well as environmental phenomena like the eroding process, rainfall rate, and particle transportation, all contribute to the introduction of sediment into reservoirs, which has an impact on the overall quality of reservoir's water and its capability for storing at the same time (Koronkevich et al., 2019). The time the reservoir retains its water and storage capacity in proportion to the annual volume of water that charges the dam determines how much the quality of the water declines (Elhag et al., 2019). From the standpoint of its optical properties, turbidity is a significant water quality metric. In both space and time turbidity fluctuates over vast waterbodies. The primary effect of particles is the modification of the water column's basic optical qualities, which include angular distribution, absorption, backscattering, and downwelling irradiance. This might impact the amount and spectrum characteristics of light or energy consumed or bounced off the top of the water. Furthermore, aquatic biodiversity, primary productivity, and the development of underwater plants may all be negatively impacted by the shift in light absorption caused by the water layer (Garg et al., 2017). Human communities built close to reservoirs greatly influence their turbidity levels and sedimentation patterns. The closest body of water is heavily impacted by these communities' fine suspended sediments, which eventually build up in the reservoir's bottom and produce muddy water (Rutherford et al., 2020). In addition to lowering the

reservoir's water quality and decreasing its capacity to store water, sediments from both natural and man-made sources can potentially trigger further natural catastrophes (Petkovšek, 2017). Secondly, increased amounts of chlorophyll-a, present in all phytoplankton organisms, often indicate a shift in the trophic status of a body of water. They are mostly linked to low biodiversity and deteriorated water quality, which negatively impact the ecosystem's services and functions (Mazhar et al., 2023). In coastal river catchments, agronomy often significantly impacts the water quality, which increases the availability and levels of nutrients in rivers. Nitrates and phosphates harm the quality of the water in the rivers and lakes they pass through (Górski et al., 2017). Since these nutrients have more time to remain in the water, the water's residence duration in the reservoirs contributes to eutrophication indirectly (Calijuri, 2002). Agronomic, manufacturing and domestic expulsions triggers cultural eutrophication, even though eutrophication is a natural phenomenon. The presence of phytoplankton in an aquatic system indicates increased primary production and increased greenhouse gas emissions. Chlorophyll, a pigment actively involved in photosynthetic processes, may be used to measure the biomass of phytoplankton (Mazhar et al., 2023). Excessive amounts of nutrients like phosphorus and nitrogen can also have negative ecological effects, such as algal blooms, lower dissolved oxygen (DO) amounts, and higher mortality among fish even though they are necessary for the survival of animals and plants (Duan et al., 2013b). Both transparency and water clarity are indirectly correlated with phosphates and nitrates and directly correlated with chlorophyll-a content (Swanson et al., 2006). Rivers that traverse diverse land use activities may include various materials and compounds, including nutrients, fallout from residential areas, total suspended sediments, and others. For example, when a river or stream flows through an agricultural region, the concentration of phosphorus load in the surface water may be larger than other characteristics. Excessive amounts of nitrogen and phosphorus in surface waters are the primary causes that endanger several biomes worldwide are agrarian runoffs

loaded with fertilizer and sewage treatment facility discharges in large quantities. Phosphates are generally carried by total suspended material (Gholizadeh et al., 2016). The overabundance of silt can cause turbidity, lower water quality, and damage ecological systems. Furthermore, catastrophic occurrences like floods can result in enormous silt accumulations that seriously impair phosphorus retention and change the distribution of nitrates (Duan et al., 2013b).

### **1.3 Laboratory Analysis and Remote Sensing of Water Quality Parameters**

Extensive data relevant to comprehending essential ecosystem attributes like physical and chemical, may be obtained by in the field measurements and recording, which serve as the foundation for long-term monitoring records required to evaluate the current state and water quality patterns. Regretfully, point-based illustrations of intricate and dynamic systems are the only ones that can be used with in situ methods (Hestir et al., 2015). Moreover, constraints that limit systematicity, including the labor-intensive and time-consuming nature of in-situ measurement, render the provision of a simultaneous regional water quality database impractical, despite its high accuracy. Moreover, for orthodox point sampling techniques it is difficult to pinpoint the temporal and geographical variabilities present in the water body, which is crucial for carefully gauging and managing them. For the management and monitoring of water quality, chronological and cohesive sampling and the challenges associated with them pose a serious threat (Duan et al., 2013; Duan et al., 2013b).

Waterbodies and extensive areas with qualitative problems may be identified and monitored more effectively and efficiently thanks to remote sensing tools. For computer handling, the digital format in which remotely sensed data is collected makes it simple to interpret. Since the 1970s, remote sensing techniques have been widely employed in the modern world to assess water quality (Gholizadeh et al., 2016). Various sensors installed on platforms (airplanes) and satellites measures the amount of radiation at different wavelengths reflected off the water's surface. Various water quality indicators, including turbidity, pH, EC,



nitrates, and chlorophyll-a content, may be found directly or indirectly using these reflections. Water quality monitoring and evaluation depend heavily on the continuum characteristics of contaminants and water, which are products of water's chemical, biotic, and hydrological properties, among other variables (Seyhan et al., 1986). Remote sensing tools can provide data for the spectral reflectance approach. Turbidity and other minerals in lake water combine to produce a body of water's brightness in optical remote sensing. Lake-to-lake variations occur in spectral regions appropriate for turbidity and Chl-a assessment, just as in minerals and other components. Several research have looked at and reported on this reflectance variance. A model's appropriate spectral channels are chosen by contrasting the estimated values with measured values acquired using a lab technique (Dall'Olmo et al., 2006). The excavation effects may be evaluated using satellite-borne photographs, and turbidity currents can identify flat-bed patterns in reservoir bottoms (Garg et al., 2017). Because it can be seen in satellite photography, chlorophyll-a is our reliable source for water quality and may also be used as an indicator of the existence of an algal bloom. Many bio-optical processes have been formed using different band combinations to recover chlorophyll-a's concentration in inshore waterways (Mishra et al., 2012). Radiation in satellite remote sensing must traverse vast amounts of the atmosphere. The radiation's strength and direction are altered along its journey because of atmospheric phenomena including dispersion and absorption from various atmospheric molecules. Therefore, the atmospheric impacts should be eliminated before utilizing the data to estimate the parameters related to water quality (Murugan et al., 2016).

As a conventional technique, multispectral remote sensing has been a main mode for classifying water quality in recent years. These days, multispectral imagery analytic techniques for quantitatively determining water quality parameters are costly and time-consuming, although producing generally reliable findings. Due to practical demands for both time- and money-saving quantitative analysis of water quality indicators and classification of the water

quality level, another hyperspectral remote sensing technology has emerged very swiftly (Harvey et al., 2015). High-frequency resolution (hyperspectral) remote sensing allows for precise measurements of the environment properties and operations by providing evaluations among thousands of distinct ranges, producing connected wavelengths that facilitate the recognition of topographic materials (Hestir et al., 2015). Thus, finer-scale spectrum patterns may be identified thanks to the advancement of hyperspectral radiometry, which increases the capacity of ocular radars to handle water's biodiversity issues like algal abundance and composition (Goyens et al., 2022).

To classify the water's quality or evaluate the significance degree of factors associated with it there are many different approaches by using remote sensing. These approaches mainly encompass machine learning, semi-analytical, and empirical techniques to measure water quality constraints and categorize the degree of water quality using hyperspectral records (Zhang et al., 2020). Above-water sensors need relatively little labor and offer high temporal resolution water reflectance data when installed on automated pointing systems. The primary motivation behind the creation of these systems was the verification of satellite data. However, to efficiently monitor water quality autonomous sovereign procedures may also be utilized due to their extremely high temporal resolution data (Goyens et al., 2022).

#### **1.4 Spectral Response of Water Bodies**

Satellite remote sensing equipment may optically measure water turbidity as it enhances light backscattering. In fact, the kinds, quantities, and presence of many elements and chemicals in water significantly impact the transmission, absorption, and reaction of electromagnetic radiation (Hafeez et al., 2019). The spectral responses of objects in water are determined by the energy reflected from them at various wavelengths. The surface characteristics and their attributes may be determined by utilizing the distinct spectral response, often referred to as spectral signature, that each form of object possesses (MOORE, 1980). In

the green, blue, and red bands, clean waters often exhibit modest reflectance, whereas the NIR spectrum shows no reflection. Because they obstruct transmittance from and to lower depths, significant quantities of suspended sediments in water result in high reflectance readings in the red and near-infrared bands (A. Pisanti et al., 2022). High absorbance in the blue and red bands is owing to photosynthetic activity, while elevated reflectance readings in the green band correlate with levels of chlorophyll, as described in the Figure 1.1.

In Figure 1.2, a distinct reflection spike appears in the reflection spectrum at around 570 nm, after which it progressively drops. It peaks again at around 706 nm. The curves exhibit less variety as the wavelength approaches 730 nm. The poor absorption of algal pigments or the dispersion of inorganic suspended materials and phytoplankton cells may be the origin of the reflectance peak at 570 nm, according to prior research. The highest absorption of chlorophyll-a in the red band may be the reason for the absorption valley between 670 and 686 nm. The luminescence of Chl-a might cause of the other reflectance peak at about 706 nm. The reflectance curves' overall shape and are comparable to those of ordinary turbid water, as described in the image below (Huang et al., 2010).

Figure 1.3 shows low reflectivity (<2%) between 400 and 450 nm in the reflectance spectra. This results from both the attenuation of colored dissolved organic matter (CDOM) and chlorophyll absorption. The poor absorption of algal pigments and the significant scattering by all particulate matter are the causes of the reflectance peak at 570 nm (>3%). Water absorption causes a wavelength drop between 670 and 675 nm. The florescence effect of Chl-a is responsible for a peak around 700–705 nm. A rise in chlorophyll is connected with this peak's migration towards longer wavelengths. Water absorption accounts for the low reflectance observed after 750 nm (Murugan et al., 2016).

In Figure 1.4 The reflection peak in the green area was highlighted by the significant absorption seen in all of the curves at the red and blue spectrum regions. The peak at the beginning of the near-infrared (NIR) (area associated with red edge), at around 710 nm to 720 nm, was another finding linked to the presence of Chl-a. At 810 nm, a different reflected characteristic linked to organic materials and chlorophyll was noticed. Apart from the Chl-a characteristics, each Rrs spectra showed a prominent absorption signature between 620 and 630 nm, which is linked to the existence of phycocyanin, a pigment found in cyanobacteria. The fluorescence of phycocyanin was connected to the reflectance peak at around 650–660 nm. One of the properties of phycocyanin is that it absorbs less in blue and green areas (Watanabe et al., 2015).

### **1.5 Significance of the Study**

Chemical alterations brought about by damming modify the water's physical and chemical qualities, which impacts water's physical and chemical qualities, which impacts nearby wetlands and rivers downstream. It is also the primary source of water for homes, which may have adverse health effects on residents. Second, at the watershed level, a sizable sample size is needed to test the quality of the water, a need that may be satisfied by using remote sensing applications. In the absence of ground data, it aids in determining the fundamental elements of water quality. Thirdly, it may be costly, time-consuming, and labor-intensive to check water quality using traditional methods. A more economical and successful option for these techniques is remote sensing. Finally, to examine the water quality and to monitor its condition in hard-to-reach places remote sensing may be used to detect pollution events or algal blooms early on. This may make prompt mitigation and intervention possible.

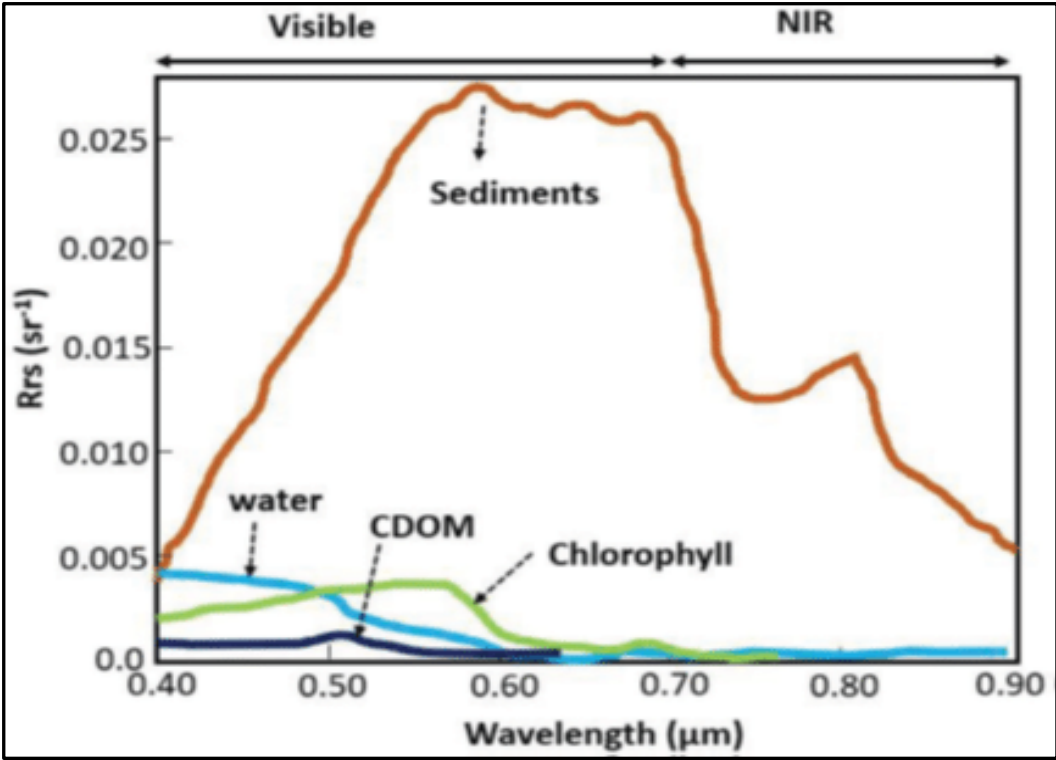


Figure 1.1. Spectral response of different elements in clear water body.

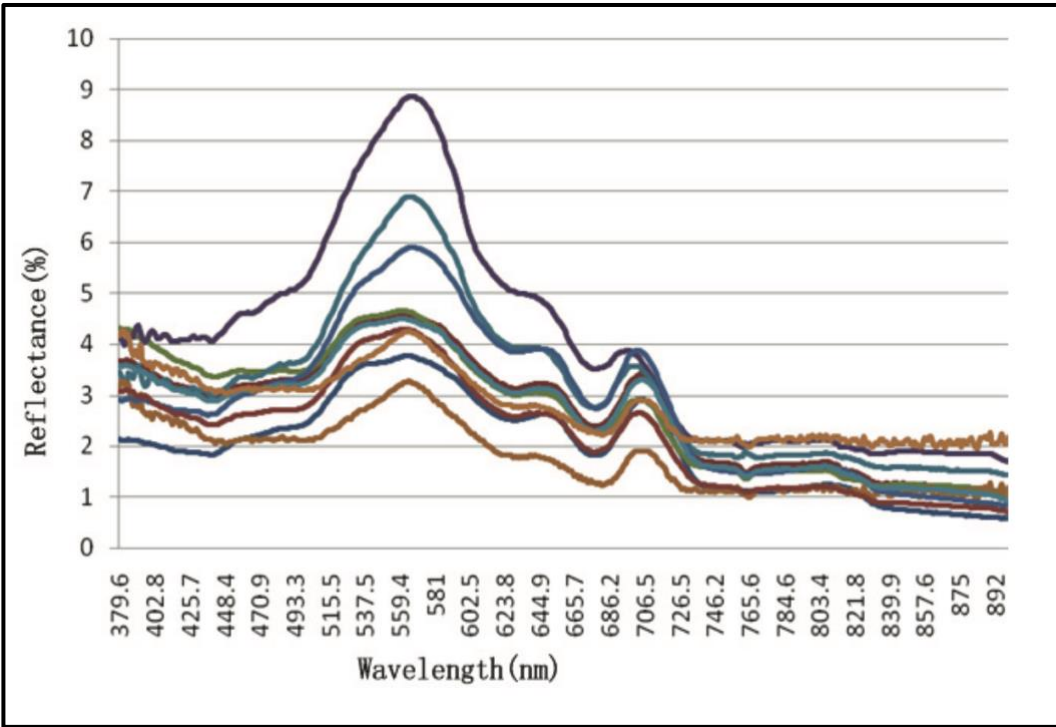


Figure 1.2. Spectral response of Tangxun lake, China.

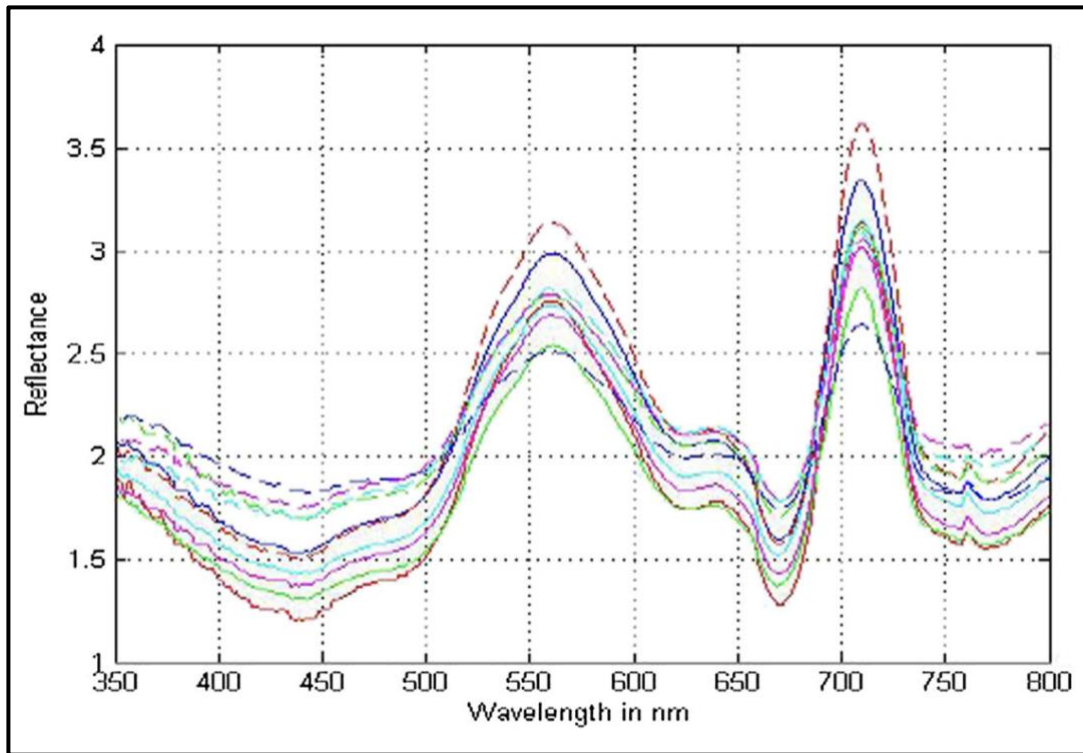


Figure 1.3. Spectral response of Krishnarajapuram lake, Bangalore.

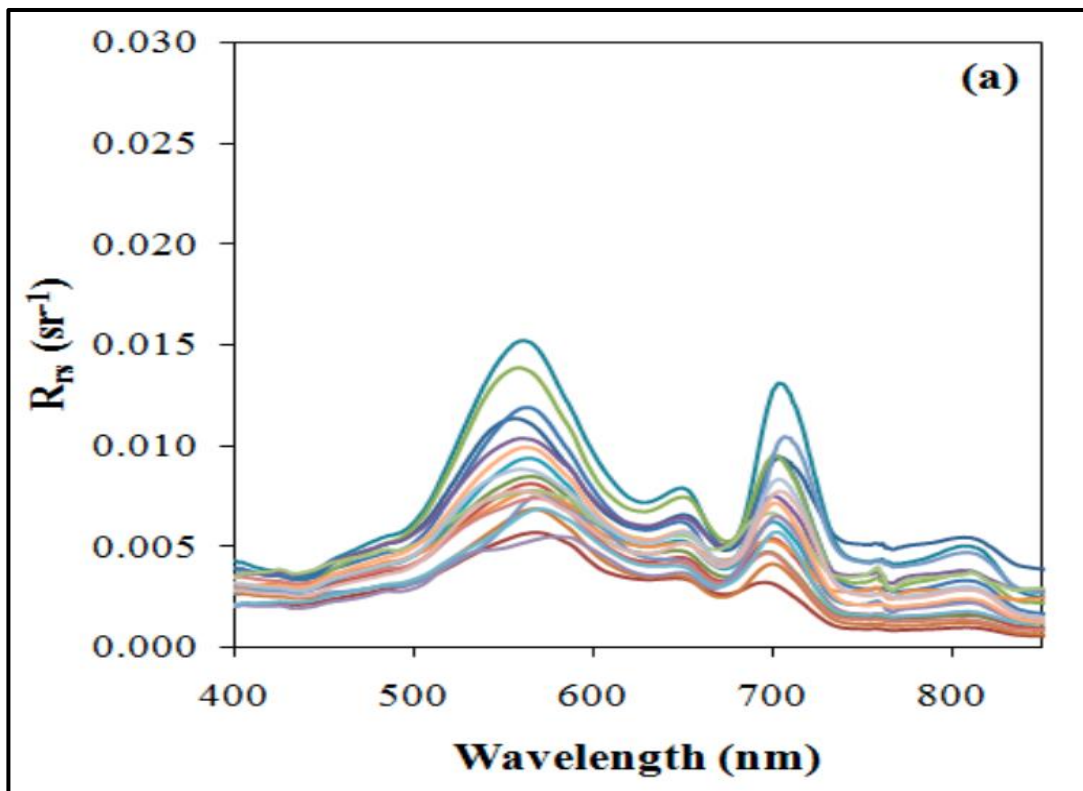


Figure 1.4. Spectral response of Barra Bonita hydroelectric reservoir.

## **1.6 Research Gap**

- Limited researches have been performed to model relationships between water quality parameters and Hyperspectral data.
- Previous studies in Pakistan didn't include Landsat multispectral data for comparison with the hyperspectral data.

## **1.7 Objectives**

The following were the objectives of the study:

- To analyze water quality parameters (pH, EC, Turbidity, Nitrates & Phosphates) of Khanpur Dam.
- To generate the multivariable statistical model using ASD hyperspectral spectroradiometer and multispectral Landsat data, with physiochemical parameters of water quality.

### LITERATURE REVIEW

#### 2.1 Water Quality Modeling in Pakistan

Iqbal et al., (2014) conducted the study in Khanpur Lake, Pakistan to evaluate the risk assessment, source allocation, and seasonal fluctuations of heavy metals in its suspended sediments. Flame atomic absorption spectrophotometry is used to assess the amounts of heavy metals in mixed specimens. Fe and Mn had high levels, whereas Cd had lowest values. PCA and cluster analysis show the primary human caused inputs of Cd, Pb, Cr, and Zn. The lowest impact values of the sediment quality standard are not met by the computed quantities of Pb, Cr, Mn, and Cd in the deposits. Furthermore, according to the ERM ratio, the sediments have a 21% chance of contamination.

One of Pakistan's largest water reservoirs, Mangla Dam, is utilized for electricity generation, agriculture, and consumption. This study evaluates the physical and chemical features and specific metals in water samples taken from the Mangla dam to determine the water's suitability for irrigation and consumption. A flame atomic absorption spectrophotometer was used to measure their concentration. Substantial anthropogenic involvements of Cd, Pb, Ni and Cr which were above tolerable limits, were demonstrated using multivariate statistical techniques in water samples from the reservoir. The pH, TDS, TA, EC, Cl<sup>-</sup>, Mg/Ca, KR, PI and PS measured values were all within allowable bounds. The water samples were classified as somewhat hard depending on the TH, yet they were deemed unfit for agricultural usage relying on HCO<sub>3</sub><sup>-</sup> and RSBC results. Future planning and management techniques were recommended to target metal pollution to restore the reservoir's water quality (Saleem et al., 2015).

Khan et al., (2018) conducted the research in Khanpur Dam, Pakistan to investigate its water quality features. Water samples were gathered from the dam's midsection, runoff,



agricultural, and society during the pre- and post-monsoon seasons. Standard techniques were employed to determine the physicochemical characteristics. The pH levels varied between 6.1 and 7.2, the conductivity between 448 to 507  $\mu\text{S}/\text{cm}$  and 363 and 505  $\mu\text{S}/\text{cm}$ , the total dissolved solid levels between 240 and 270 mg/L, the chloride levels between 10.635 to 26.5875 mg/L and 17.725 to 53.175 mg/L , and the fluoride levels between 0 and 2.4 mg/L. The samples' levels of heavy metals were also evaluated using a conventional procedure and an atomic absorption spectrophotometer. The Pak-EPA standard limit was compared to the obtained findings. It was discovered that most post-monsoon samples had concentrations of heavy metals (such as nickel, cadmium, chromium, and lead) and fluoride were higher than allowed. Before its supply, regulatory bodies and relevant agencies should keep an eye on the water quality.

An innovative method of judging water quality is the water quality index (WQI). However, most of the indices are not relevant to all types of water since they rely on fundamental physio-chemical water characteristics, which can cause them to be biased and sensitive to certain features. These variables include time, location, sample frequency and quantity, and variable weight assignment. Five WQIs were computed for two temporal periods in the current study: Data acquired in real-time from June to December using Internet of Things nodes at Rawal Dam's entrance and exit streams. Using GIS-based grab sampling from 2012 to 2019 data was collected from the Rawal Dam Water Filtration Plant. The compiled datasets were classified as Very Poor by the calculated WQIs. Furthermore, this study looks at how machine learning algorithms may be used to classify water quality. With a 99% accuracy in classification, the analysis statistics demonstrated that the DT method functioned better than the rest of the models. Even though WQI is a broadly used technique for estimating water quality, it is important to consider the prejudices and ambiguities brought about by the constraints of data collection that result in class imbalance (Ahmed et al., 2021).

The depletion of freshwater reservoirs can have negative consequences on water quality due to overexploitation and insufficient upkeep. In this work, the initial evaluation of the water's cleanliness and ecological circumstances in Pakistan's Khanpur reservoir is conducted through the practical retrieval of two transparency markers, TSS and Secchi disc depth (SDD), using Sentinel-2 satellite imagery. To understand the behavior of water transparency trends in the created reservoir spatially and temporally, the study used two separate designs (semiempirical remote sensing algorithms and regional coast color ANN-analytical neural network model). Three of the five months that were analyzed have excessive turbidity and poor eutrophic conditions in the reservoir water. When the outcomes of the two computer models are compared, there is a strong statistical correlation. This technique is especially helpful in areas lacking regular ground sampling and ecological parameter monitoring (Faizi et al., 2022).

Muhammad et al., (2022) conducted the study on the Gomal Zam Dam and its branches in south Waziristan District, Pakistan. The study examined the water's condition and seasonal variations in the area. Water samples were taken for this reason in both summer and winter from Dam and its associated rivers. Except for turbidity, water samples were determined to be within the World Health Organization's (WHO) secure drinking water limits. Because of increased pollution, the water quality is somewhat worse in the winter than it is in the summer. The corrosion of foundation was the primary characteristic of the water quality of Dam. In the summer and winter, the investigated water is categorized as Mg-HCO<sub>3</sub> type and Na-Cl type, respectively. Geogenic causes of rock weathering mostly control the area's water quality. According to statistical assessments, the area's water quality is mostly controlled by geogenic causes of rock weathering.

Akbar et al., (2022) conducted the research in of the Rawal and Khanpur Dams to gauge their microbiological characteristics and water quality. 5 sampling locations were selected. Conventional approaches were used to test a variety of physico-chemical limitations. The

amounts of heavy metals were evaluated using atomic absorption spectroscopy. Using the SPC technique the total coliform count and total viable count in water samples were determined. Water samples were used to isolate distinct bacteriological colonies, which were then identified by Gramme staining test. Numerous physicochemical parameters were found to be within WHO criteria. However, several samples had higher conductivity ratings than the WHO allowed. The Rawal Dam was confirmed to provide safe drinking water, except a few areas where elevated microbiological counts were discovered. To guarantee that customers receive safe water to consume, more research on water quality is necessary.

Globally, human activities have a significant impact on lake ecosystems. The effects of human activity are most noticeable when it comes to light, nutrients, and deposition. The purpose of this research is to investigate how the water quality of Tarbela Reservoir changed amid 1990 and 2020. LULC, NDCI, NDTI, and NDWI in Tarbela Reservoir and its environs were observed using Landsat images. The built-up area in the reservoir's western and eastern regions has significantly increased, according to the data, but the turbidity level has decreased a 4% drop over the past ten years, confirming the water quality improvement. Also, the research showed the water extent water and chlorophyll indexes, indicating a rise in the water's residence duration. It is determined that although the water condition declined over the years, the dam's overall water quality improved and its ecology recovered in 2020 (Mazhar et al., 2023).

## **2.2 Remote Sensing of Water Quality Assessment Across the Globe**

Senay et al., (2002) conducted the study to assess of the temporal and geographical variability of optical water quality measures, containing turbidity, TSS, and chlorophyll a, in the Greater Miami River, Ohio, that has been accomplished with effectiveness through remote sensing data. Aerial hyperspectral detectors, a laboratory spectrometer, and a portable spectroradiometer were used to gather spectral data in the summer of 1999. On the same days

as the cross-section, observations of water quality variables, including turbidity and chlorophyll concentrations were taken. A handful of wide spectral bands and ocular water quality measures were shown to correlate. A further, theoretically more robust association between a water quality measure and nearby wave zones is represented by derivative reflectance. There is a high correlation between the ratio of wavebands 705 and 672 and turbidity with  $R^2 = 0.79$  and chlorophyll a with  $R^2 = 0.7$ , and the first derivative of wavebands 700 and 675. These connections made predictions of turbidity and chlorophyll concentrations in areas of the Greater Miami River where only hyperspectral data were collected possible. Maps of the relative distribution and turbidity of chlorophyll were created using hyperspectral photos of the river.

To assess how humic colour affected satellite-inferred water quality conditions, researchers employed Landsat TM data from the same lakes and ground-based observations on 15 lakes in Minnesota with a variety of optical characteristics. Except at extremely high levels ( $> \sim 300$  chlorophyll a units, CPU), colour (C440), as determined by absorbance at 440 nm, only slightly biases estimations of Secchi disc transparency (SDT) using Landsat TM data. Similar to this, low-to-moderate levels of humic colour have no effect on the association between SDT and chl a concentration when chlorophyll a (chl a) levels are moderate or high ( $> 10 \mu\text{g/L}$ ), but they have a significant effect at high levels of C440 (e.g.,  $> \sim 200$  CPU). On the other hand, when chl-a levels are low, departures from the overall Chl a-SDT connection happen at significantly lower C440 values ( $\sim 60$  CPU). Strong statistical correlations were discovered between the observed brightness of several Landsat TM bands and the optical characteristics of lake water, which are often linked to algal abundance (SDT, Chl a, turbidity). Based on  $R^2$  and the lack of statistical outliers or lakes with significant leverage, combinations of bands 1, 2, or 4 with the band ratio 1:3 ( $R^2 = 0.88$ ) showed the best associations for chl a. Multiple regression analyses between  $\ln(\text{C440})$  and combinations of bands 1-4 and band ratios

produced several relationships with  $R^2 \geq 0.70$ , suggesting that C440 can be estimated with fair reliability from Landsat TM data, despite the fact that TM bands 1-4 alone or as simple ratios were poor predictors of C440 (Brezonik et al., 2005).

Lin et al., (2009) conducted the research on the largest freshwater lake called Baiyangdian Wetland, in northern China. This area's water quality has been declining recently. At Baiyangdian Wetland, 67 water quality samples were taken in September. The variables measured were pH, DO, chlorophyll-a, blue-green algae, and total dissolved solid. The outcomes of the assessment indicate that Baiyangdian Wetland was severely polluted. The northern region has a greater amount of chlorophyll than the southern region. A field spectroradiometer (ASD FieldSpec) was used to simultaneously gauge the water upwelling radiance at eighteen sample points. By contrasting the spectrum profiles of water and the amount of chlorophyll, it was discovered that the reflectance maxima decrease in the 560–575 nm range as chlorophyll levels rise. Reflectance maxima grow at the band scope of about 700 nm as the levels of chlorophyll rise. The correlation coefficient for chlorophyll shows that the maximum positive correlation is 0.9133 for the 722 nm band. There is an adverse association between the bands at 550 nm and 670 nm and an upward trend between the bands at 700 nm. Using data from remotely sensed sensors, these bands can be selected to recover chlorophyll saturation.

The aim of this research is to evaluate how well hyperspectral metrics can identify Chl-A intensities in Tangxun Lake, China. Reflectance ratio, the first derivative of reflectance, and single-band reflectance, three different types of hyperspectral methods were recovered. The outcomes of the assessment showed a strong correlation ( $R^2 > 0.8$ ) between the observed amounts of Chl-a and both techniques: the reflectance ratio and the first derivative of reflectance. Thus, these hyperspectral techniques might be a handy way of recording both temporal and geographic fluctuations of Chl-a accumulation (Huang et al., 2010).

Wu et al., (2014) carried out the study to reveal the importance of total suspended solids as water quality indicator. A spectroradiometer was used in this investigation, and a few water quality measurements were examined both at the research locations and in the lab for additional examination. The findings of the water quality were connected. Additionally, data was modelled using artificial neural networks and multiple-regression. The findings showed a substantial positive correlation between TSS and turbidity throughout the wavelength. The 700 and 900 nm 700 and 900 nm regions are where the best wavelengths are discovered for measuring turbidity and TSS, respectively. However, by applying MR, the ANN technique can enhance the TSS retrieval. Because the transformation model is nonlinear, the precision of the TSS estimate using ANN is  $R^2 = 0.66$  was superior to that of the MR technique ( $R^2 = 0.58$ ).

Water quality is gauged by algal quantity, obtained by estimating the Chl-a content. Using an analytical approach to estimate Chl-a requires a lot of labor and reagents. However, spectral reflectance techniques such as satellite remote sensing and in-situ hyperspectral spectroradiometer studies are less costly and yield quicker outcomes. This study aims to quantify the amount of chlorophyll-a by using data from Landsat-7 (ETM+) and hyperspectral spectroradiometers. To ascertain the correlation between quantified levels of Chl-a and band reflectance ratios regression model was used. It was discovered that spectroradiometer data, as opposed to multispectral data, offered a stronger connection with observed levels of Chl-a. Since satellite data offers complete coverage, it was used to map the lake's content of Chl-a (Murugan et al., 2016).

The eutrophic level is raised by excessive nutrient concentrations and water retention time. Eutrophication and phytoplankton primary productivity are directly connected. There may be issues with public health if these species are present in large quantities. Therefore, mapping chl-a present in these species using remote sensing is practical substitute. This study aimed to assess how well Landsat 8 (OLI) satellite photos performed in identifying Chl-a levels

and calculating the eutrophication level in a humid reservoir. Data for fitting experimental models, 2 field visits were performed in May and October of 2014 provided. A temporal sequence of OLI pictures was subjected to model application. The atmospheric correction most certainly hindered the performance of the Chl-a concentration models, even though they produced respectable findings. Therefore, better results were not achieved by categorizing trophic levels (Watanabe et al., 2015).

Elhag et al., (2019) carried out the research on Wadi Baysh dam, Saudi Arabia for water quality analysis. The water quality metrics of nitrate levels, chlorophyll levels and turbidity were employed. Over two years, water quality measurements were gathered daily from the water treatment plant near the dam and subsequently compared to those measured remotely. Sentinel-2 was used to gather remote sensing data. The MCI, GNDVI, and NDTI were estimated using data processing. The regression analysis between the non-spatial data collected from the water treatment plant and the spatial data inferred from the remote sensing photos was enhanced by applying zonal statistics. Real-time readings of chlorophyll showed a strong association with MCI values ( $R^2 = 0.96$ ), real-time levels of nitrate demonstrated a significant relationship with GNDVI values ( $R^2 = 0.94$ ), and real-world water turbidity observations demonstrated a strong connection with NDTI values ( $R^2 = 0.94$ ). The study results provide credence to the estimation of water quality variables in dry situations using Sentinel-2 remote sensing data.

The amount of nutrients in coastal water has increased dramatically over the past several decades, causing an overabundance of algae bloom. The number of algae is frequently determined using chlorophyll-a as a marker. This research aims to track the amount of chlorophyll-a in Dubai Creek using WorldView-2 imagery and investigate the correlation between chlorophyll-a and other eutrophication indices. With interposed ground levels of chlorophyll-a, a spectral model of the WorldView-2 multispectral picture was used to monitor

the concentration of chlorophyll-a. The model produced an R2 of 0.82. The reliability of the WorldView-2 model was demonstrated using Landsat 7 (ETM+) pictures, which addressed the temporal gap between the image and ground data. A different model that was created to show the connection between total nitrogen and orthophosphate levels and spectral chlorophyll-a levels had an R2 of 0.97, indicating strong agreement. Additionally, it was discovered that the produced models may be used for identifying orthophosphate, total nitrogen, and chlorophyll-a minus the requirement for expensive on-site data collection procedures (Mortula et al., 2020).



### MATERIALS AND METHODS

#### 3.1 Study Area

Situated on the Haro River in the Haripur district of Khyber Pakhtunkhwa province, Khanpur Dam is a sizable multifunctional structure (Figure 3.1). The Haro River traverses portions of the Khyber Pakhtunkhwa and Punjab states. Lora Haro and Stora Haro empty it after it flows from Changla Gali and Nathia Gali. While the Stora Haro falls from the slopes of Nathia Gali, the Lora Haro flows through the Murree slopes. The Lora Haro becomes Stora Haro at Jabri. The Haro River is dammed in Khanpur after flowing through steep, tight canyons. Early in the 1980s, a reservoir was constructed. The Khanpur Dam was designed to store water for irrigation, supply potable water to the downstream twin towns of Rawalpindi and Islamabad, and supply power to the Taxila manufacturing complex (Nauman et al., 2019). The springs and streams meet the residential water supply throughout the year. Given its 1,06,000-acre feet of overall space for storage, the dam is regarded as big in terms of its ability to store water. The dam has had several difficulties recently, such as siltation and reduced water supply due to climate change and rising water demand. Additionally, the release of unprocessed commercial and household wastewater into the Haro River, which feeds into the dam, contributes to the river's rising pollution. When drinking water and using it for other household needs, the water quality in the dam is impacted, which may have negative health effects (Mir, 2022). Ariel photograph of the dam is shown in Figure 3.2.

#### 3.2 Brief Description of Methodology

Figure 3.3 shows methodology flow chart. Firstly, in-situ water quality measurement was done using hyperspectral spectroradiometer by recording its spectra. Secondly, surface water samples were collected from the exact location in dark water bottles (500ml) and then its

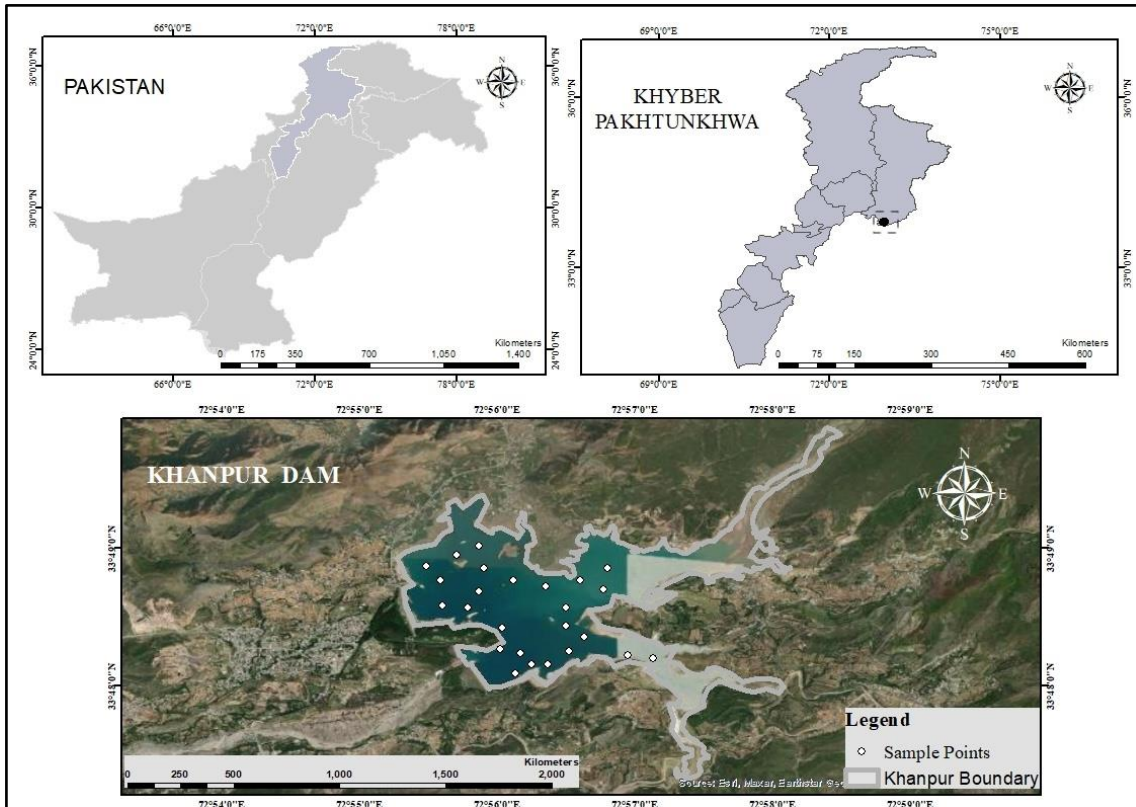


Figure 3.1. Study area.



Figure 3.2. Khanpur dam ariel photograph. (Source: [https://twitter.com/amazing\\_pk/status/947384075156885504](https://twitter.com/amazing_pk/status/947384075156885504))

physiochemical parameters were analysed in the laboratory. Furthermore, Landsat 8 image was downloaded from the USGS website and its pre-processing parameters were applied using ENVI software. Then different spectral indices (chlorophyll index to check eutrophication, turbidity index to check suspended solids amount) were applied. A statistical multivariate model was developed to predict the water quality parameters using remote sensing (Landsat & ASD Hyperspectral data) and allied water quality parameters. Lastly, root means square error (RMSE) metric is applied on results for model validation. Table 3.1 describes the dataset characteristics, like the source and specifications of the data used in the study.

### **3.2.1 Field Water Sampling**

Prior to entering the field, a sample guideline was made in which the following details were recorded: date, time, location, number and summary of the spectroradiometer recordings, and coordinates. On July 11, 2023, sampling was conducted under sunny conditions (Figure 3.4). The essential physical attributes were recorded in a table. After that, an appropriate sample was done. At the Khanpur Dam, 25 water samples were taken at various locations. Firstly, ASD spectroradiometer was used to collect the data in a vertical downward orientation above the water's surface. Two of these devices were used: one to gather the water's upwelling brightness and the other to gather its downwelling radiance. The water body's upwelling radiances were recovered with about 100% reflectivity throughout the whole spectrum. The ratio of downwelling irradiance to upwelling radiance coming from the water's surface is known as reflectance. For every sample, ten distinct sets of scans were measured. Above the water's surface the probe was manually held at 0.5 m and pointed vertically downward towards the water, and around 1m away from the boat during the spectra measurement. After arriving at its new place, the boat was halted for 1 minutes before taking measurements to even out the waves and ripples.

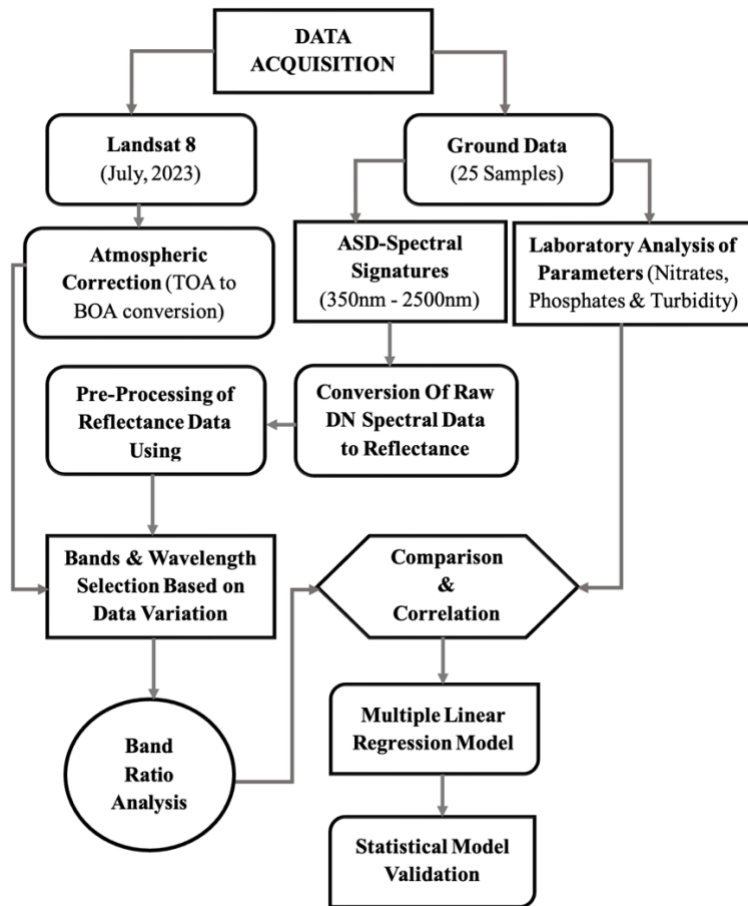


Figure 3.3. Methodology flow chart

Table 3.1. Dataset characteristics.

No.	Data Type	Specification	Source
1.	Satellite Imagery	Landsat 8 (OLI) 30 m spatial resolution	USGS
2.	Hyperspectral data	ASD spectroradiometer (220nm-2500nm)	Field samples
3.	Water Quality parameters	pH, EC, turbidity, nitrates, phosphates	Field samples & laboratory analysis

Since the spectroradiometer was positioned less than two meters from the water's surface, air dispersion and light absorption effects were deemed insignificant. Following spectrum measurements, surface water samples were taken vertically and collected with 500 ml dark polyethylene water bottles at a depth of 50cm. The sample process was carried out carefully. The bottles were then promptly sealed by placing the lid on top of them. Bottles were then dried after their thorough cleaning. In order to prevent contact with sunshine, specimens were promptly stored in an ice box. After the sample collection was completed, samples were analyzed for different parameters. The sampling location's coordinates are given in table1-A in appendix.

### **3.2.2 Laboratory Analysis**

Physiochemical parameters like pH, EC and Turbidity were examined in the Institute of Environmental Sciences and Engineering (IESE), NUST laboratory (figure 3.5) and for the examination of other parameters like nitrates and phosphates samples were sent to the Pakistan Council of Research in Water Resources (PCRWR) laboratory. Table 3.2 describes the permissible limits set by WHO and Pak-EPA for these parameters.

#### **3.2.2.1 pH**

A cylindrical piece of glass containing a layer of hydrated gel, an analog electrode, a standard solution, and a reference connector make up a pH electrode. The electrode generates a current that measures the difference in charge between the solution inside the bulb and the solution outside the gel layer after it is immersed in the sample. For analysis, firstly, pH meter was calibrated using three different buffer solutions and then pH of every sample was recorded by using the pH meter and washing it with distilled water after every sample analysis to achieve more accurate results.

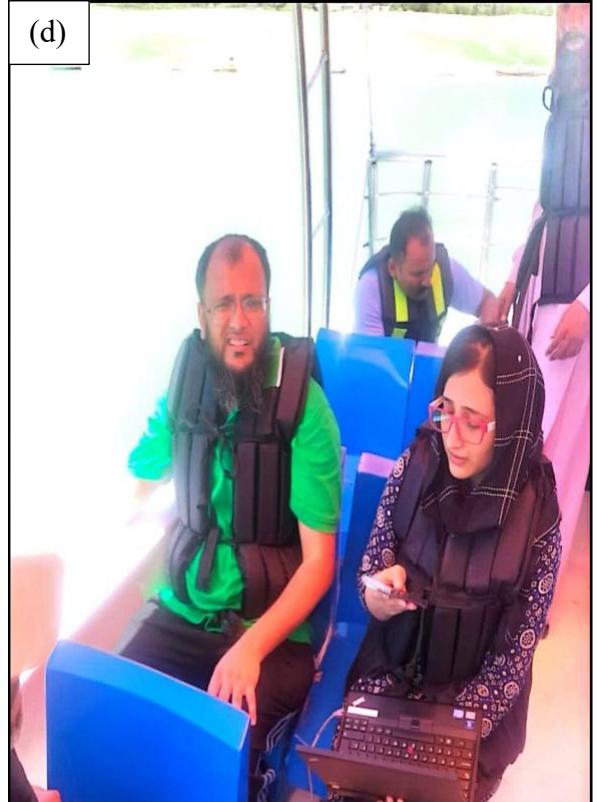
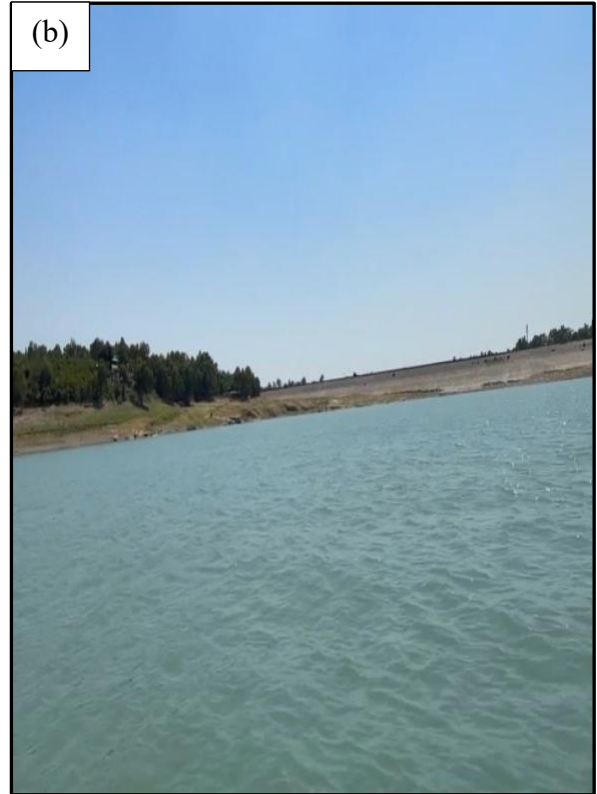


Figure 3.4 (a, b, c, d) Field sampling

### 3.2.2.2 EC

For EC measurement of water samples two electrode probe EC meter was used, which was built such that both probes would come into simultaneous touch with the sample and were composed of non-reactive material. Higher EC readings are obtained when more ions are present in the sample because these two electrodes transmit a current at a specified frequency. During the analysis EC meter was washed with distilled water after every recording for better results. Micro Siemens per centimeter ( $\mu\text{S}/\text{cm}$ ) and milli Siemens per centimeter ( $\text{mS}/\text{cm}$ ) are the units used to measure conductivity.

### 3.2.2.3 Turbidity

Similarly, the turbidity meter was calibrated first, using standards of known turbidity. The water sample that is to be examined is put into a clean cuvette. The device measures the amount of light scattered after exposure to a water sample; the amount of scattering is directly related to the sample's turbidity. The device gives a reading in nephelometric turbidity units (NTU).

### 3.2.2.4 Nitrates

While the PCRWR conducted nitrate analysis of water samples, the overall experimental procedure for their examination is outlined as follows:

- A  $50\text{ cm}^3$  volumetric flask was pipetted with  $0\text{ cm}^3$  of the water sample.
- After adding and whirling  $10\text{ cm}^3$  of 13N sulfuric acid, the flask was left in a cold-water bath ( $0\text{--}10$ )  $^\circ\text{C}$  to reach thermal equilibrium.
- After adding and diluting  $0.5\text{ cm}^3$  of brucine-sulfanilic acid to the mark with deionized water, the solution was heated to  $100^\circ\text{C}$  for approximately 25 minutes to maximize color development.
- The flask was then allowed to cool to room temperature. Including the blank, the absorbance was measured at 410 nm using UV-spectrophotometer.

- These steps were repeated for all samples (Sa'id and Mahmud, 2013).

#### 3.2.2.5 Phosphates

Similarly, phosphate analysis of water samples was done by PCRWR, a general experimental procedure is as follows:

- After pipetting 50 cm<sup>3</sup> of water sample into a 500 cm<sup>3</sup> volumetric flask, 3.0 cm<sup>3</sup> of ascorbic acid and 5 cm<sup>3</sup> of ammonium molybdate solution were added while swirling.
- The mixture was then diluted with deionized water to the appropriate level and left for 30 minutes to allow for the maximum development of color.
- The absorbance was then measured at 660 nm, including the blank using UV-spectrophotometer.
- Steps will be repeated for remaining samples (Sa'id and Mahmud, 2013).

#### 3.2.3 ASD-Hyperspectral Spectroradiometer Data Analysis

Spectral signatures of water samples were collected using ASD Field Spectroradiometer during the sample process. For each water sample, ten separate spectra were obtained. The integrated RS3 program was used to record the spectral signatures. The recorded signatures were in the form of ASD binary files. In View Spec Pro software these ASD files were then imported and from there these files were converted into text files. Then these text files were opened in excel and an average of ten spectra of each sample was then taken. Figure 3.6 shows the mean twenty-five raw spectral signatures collected from Khanpur dam.

Prior to building a model, the spectra were transformed by applying Savitzky-Golay smoothing with 3<sup>rd</sup> derivative and twenty smoothing points in SpectraGryph software (figure 3.7). This transformation is necessary for smoothing spectra and to remove particle size effects and noise produced due to illumination variations as stated by (Tsai and Philpot, 1996). Even after smoothing and baseline corrections only 400-950 nm of the wavelength range was used because of low signal to noise ratio over water body.



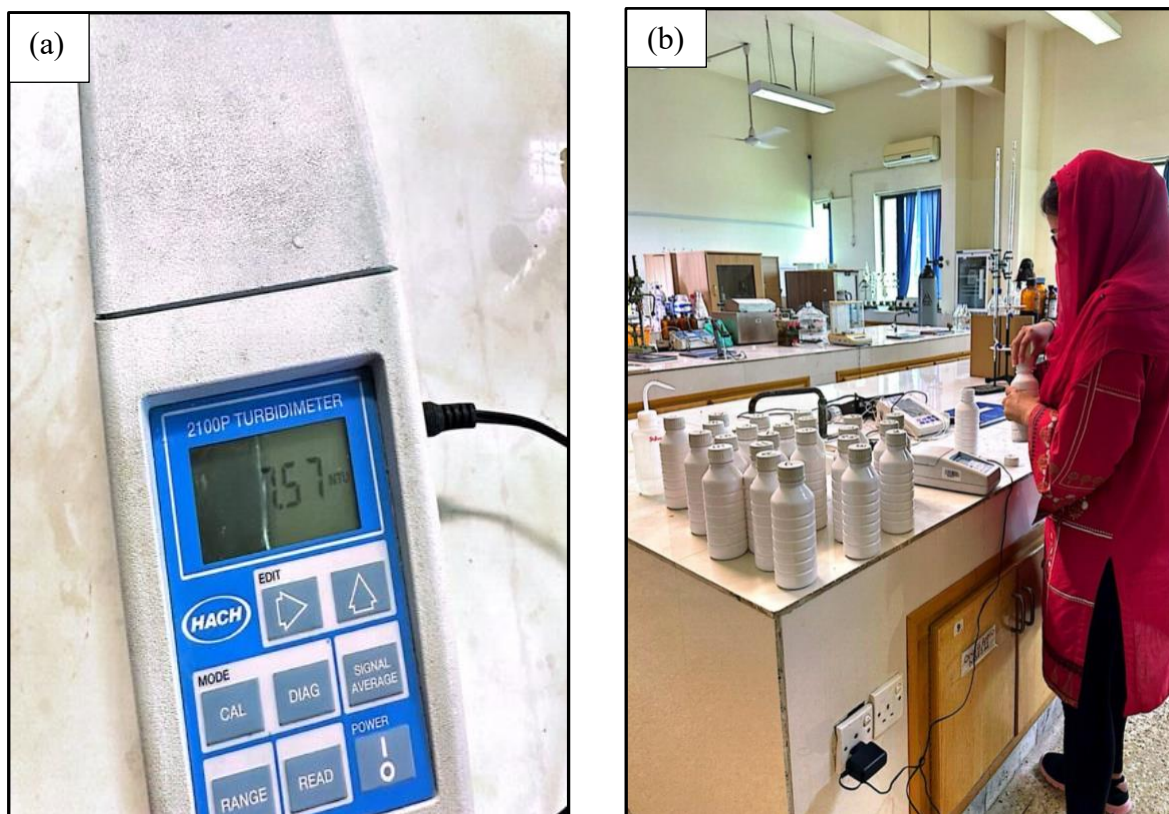


Figure 3.5. (a, b) Laboratory analysis in IESE lab, NUST.

Table 3.2. Permissible limits of water quality parameters.

<b>Parameters</b>	<b>NSDWQ</b> (National Standards for Drinking Water Quality)	<b>WHO Standards</b> (World Health Organization)
pH	6.5-8.5	6.5-8.5
EC	300-500 micro-Siemens/cm	$\leq 400$ micro-Siemens/cm
Turbidity	<5 NTU	<5 NTU
Nitrates	$\leq 50$ mg/L	<11.3 mg/L
Phosphates	0.05mg/L	NGVS (No Guideline Value Set)

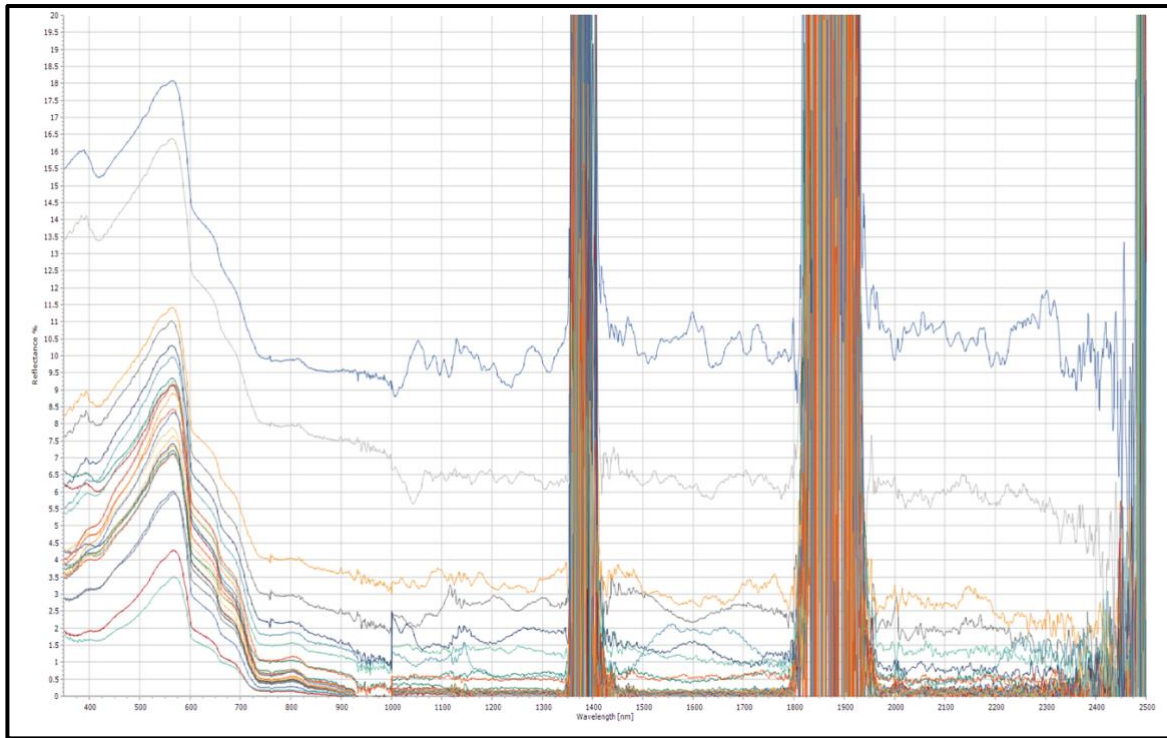


Figure 3.6. Raw reflectance signatures collected from ASD spectroradiometer.

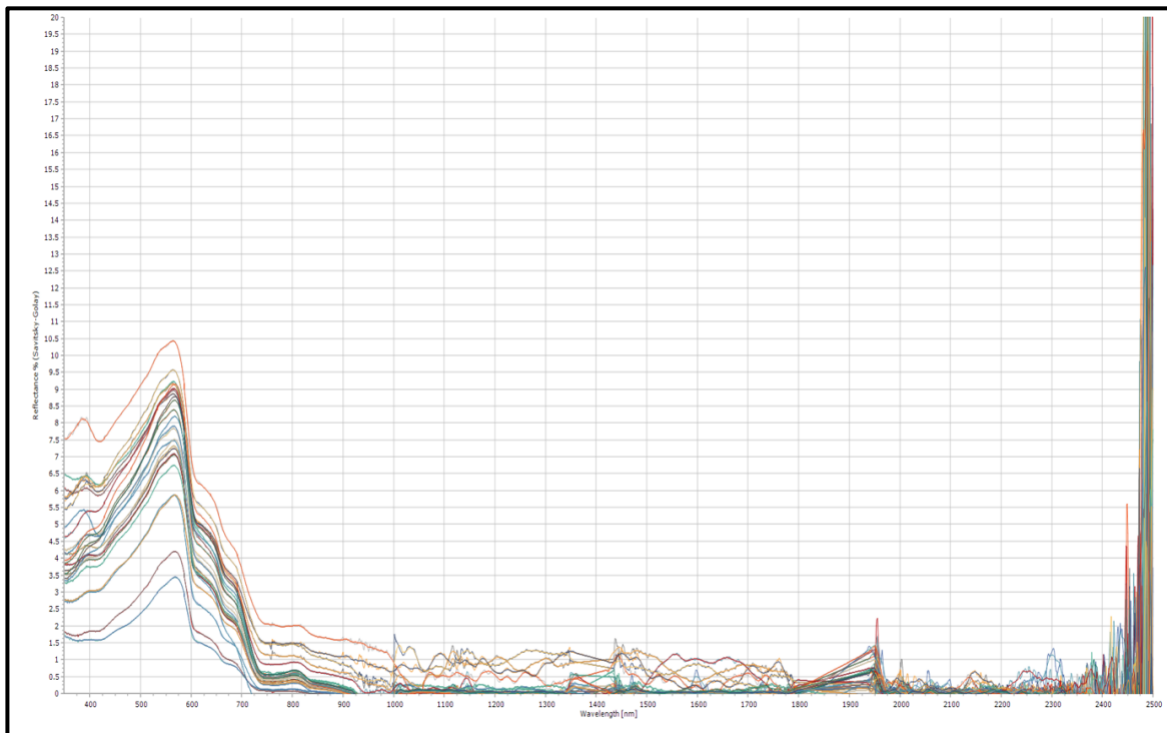


Figure 3.7. Post-processed reflectance signatures.

### **3.2.4 Multi-spectral Landsat 8 OLI Data**

With a panchromatic band providing data at 15 meters, the Operational Land Imager (OLI) sensor records images in nine spectral bands, covering the coastal/aerosol, blue, green, red, near-infrared, short wavelength infrared (SWIR), with most bands providing a spatial resolution of 30 meters. Furthermore, Landsat OLI collects thermal data with a 100-meter resolution using its Thermal Infrared Sensor (TIRS). Landsat 8 OLI Level-2, Collection-2 image of Khanpur dam was downloaded from USGS website. The image was of the same day sampling was done, for more accurate results. To get bottom-of-atmosphere (BOA) reflectance values, pre-processing of Landsat image was carried out before to analysis. Software called ENVI was utilized for this. After that, indices like the NDTI and NDCI were applied to detect turbidity and chlorophyll index which is directly or indirectly related to presence of nitrates and phosphates in the water body as they are the major contributors of eutrophication. Chlorophyll index is applied as the resolution of multispectral Landsat data is not high enough to detect presence of nutrients like nitrates and phosphates in the water. Furthermore, band ratios were chosen from this atmospherically adjusted data, and their values were extracted with the help of Arc map for each sample point. Band ratio method highlights or enhance specific geographic features based on the selected band's reflectance. Mainly green and red bands were selected for their reflectance and NIR band for its absorbance characteristics in water body, to get variable data.

### **3.2.5 Multiple Linear Regression Model**

At the end of the analysis, correlation matrix and MLR models of ASD hyperspectral spectroradiometer and multispectral Landsat data with ground data were generated. Regression is a statistical method used to model the relationship between one dependent variable and one

or more independent variables. A simple linear regression has one dependent variable and one independent variable, and the relationship is represented by a straight line (Kenton, 2022).

The equation for a simple linear regression model is often written as:

$$Y = \alpha + \beta X + \epsilon$$

Where:

- $Y$  is dependent variable,
- $X$  is independent variable,
- $\alpha$  is the y-intercept (the value of  $Y$  when  $X$  is 0),
- $\beta X$  is the slope of the line (the change in  $Y$  for a one-unit change in  $X$ ),
- $\epsilon$  is the error term (representing unobserved factors or random noise).

### 3.2.6 Model Validation

Following metrics are used for MLR model validation:

- Root means square error (RMSE) is a standard metric used to calculate the precision of regression model. It computes average magnitude of errors between actual and predicted values. The more results are closer to zero and more accurate (Tyagi et al., 2022).

$$RMSE = \sqrt{\frac{\sum_{i=1}^n (y_i - \hat{y}_i)^2}{n}}$$

Where  $n$  is the number of observations,  $y_i$  is the actual observed value and  $\hat{y}_i$  is the predicted value.

- $R^2$ : A metric that indicates how well a model fits data sets is the coefficient of determination. It is a statistical indicator of how closely the regression line resembles the real data in the context of regression. Range from 0-1, the closer the value to 1 the more accurate are the results.

- $r$ : The correlation or relationship between a dependent and an independent variable is which is expressed by  $r$  known as the correlation coefficient, in a regression analysis. It has a range of  $-1$  to  $+1$ , which shows a perfect negative or positive association between the independent and dependent variables, respectively. Consequently, the absence of a link between these variables is shown by value of  $0$  (Kasuya, 2018).
- $p$ -value: The null hypothesis that the coefficient is equal to zero (no effect) is tested by the  $p$ -value for each element. A  $p$ -value of less than  $0.05$  suggests that the null hypothesis may be rejected. Stated differently, a predictor with a low  $p$ -value will probably be a useful addition to your model as variations in the predictor's value correspond with variations in the response variable. On the other hand, a higher (insignificant)  $p$ -value indicates that variations in the predictor has no bearing on variations in the responder (Bevans, 2020).

### RESULTS AND DISCUSSIONS

#### 4.1 Results of Laboratory Analysis

Table 4.1 shows the summary statistic results of water quality parameters. Three key water quality parameters, nitrates, phosphates and turbidity, have exceeded the WHO permissible limits. It was found that concentration of phosphates ranges from 0.03 mg/L to 0.58 mg/L while, nitrates ranges from 0.39mg/L to 2.19 mg/L. Turbidity ranges from 4.36 (NTU) to 8.95 (NTU). Also, EC ranges 376 s/m to 414 s/m whereas, pH ranges from 7.28 to 8.94. These parameters' average concentration was 0.34mg/L for phosphates and 7.02 for NTU turbidity. The NSDWG prescribed limits for these parameters are <0.05 and <5, respectively. These results highlight an important deviation from the advised guidelines for these water quality parameters, which calls for prompt attention and corrective measures to address any possible risks to the public's health and the environment. While other three parameters, pH level recorded in the Khanpur Dam samples averages 7.88, aligning with the NSDWG-recommended range of 6.5-8.5. Similarly, the EC was measured at 388.48, falling below the permissible limit of < 500 and 1.22 mg/L for nitrates which are within the permissible limit of < 50. These results indicate a satisfactory adherence to the specified guidelines for pH and EC, underscoring a degree of balance in these particular facets of water quality within the studied context. Phosphates and nitrates have 0.173 and 0.529 values of standard deviation. These findings indicate that phosphates have a low standard deviation, which suggests some stability or consistency in their readings. When compared to phosphates, nitrates have a larger standard deviation, which indicates more measurement variability. Turbidity has a moderate to high standard deviation, i-e 1.396, this shows considerable variability. EC has high standard deviation of 7.633 which indicates substantial variability. Meanwhile, pH has low variability as its standard deviation is 0.340. Overall standard deviation results show that EC exhibits the

highest parameter variability. Phosphates and pH show low variability while, turbidity and nitrates fall in between. Nitrates and pH present positive skewness, specifying the existence of outliers with high values, while phosphates, turbidity and EC show negative skewness, indicating the presence of outliers with low values. EC and pH reveal high positive kurtosis, signifying the presence of extreme values, whereas phosphates, nitrates and turbidity show negative kurtosis, implying the existence of fewer extreme values.

Then the correlation matrix of these parameters was made better to understand the effect of one variable on another variable. Table 4.2 shows the correlation matrix of water quality parameters. Its shows significance at 0.05 significance level, indicated by (\*) sign. Nitrate have a strong positive correlation with phosphate  $r = 0.68$  and turbidity  $r = 0.173$  whereas weak positive correlation with pH  $r = 0.168$  and weak negative correlation with EC  $r = -0.212$ . Turbidity exhibits a strong positive correlation with phosphates  $r = 0.806$ , weak positive correlation with pH  $r = 0.108$  and weak negative correlation with EC  $r = 0.194$ . EC shows no correlation with phosphates  $r = -0.005$  and moderate positive correlation with pH  $0.472$ . Phosphates show weak positive correlation with pH  $r = 0.235$ . Overall, these results suggest that, the significant correlations indicated between nitrate and phosphate, as well as nitrate and turbidity, indicates that rising phosphate and turbidity levels accompany rising nitrate concentrations. There is a minor tendency for nitrate levels to fall as EC increases, which the weak negative association between nitrate and EC indicates. There appears to be a tendency for electrical conductivity to rise along with pH, as shown by the somewhat positive correlation seen between the two variables. Turbidity and phosphate as well as turbidity and pH have substantial positive correlations, indicating a relationship between turbidity variations and phosphate and pH variations.

Table 4.1. Summary statistics of water quality parameters

<b>Statistics*</b>	<b>Phosphate (mg/l)</b>	<b>Nitrate (mg/l)</b>	<b>Turbidity (NTU)</b>	<b>EC (s/m)</b>	<b>pH</b>
Min	0.03	0.39	4.36	376	7.28
Max	0.58	2.15	8.95	414	8.94
Mean	0.34 (< 0.05)	1.22 (< 50)	7.02 (< 5)	388.48 (≤ 500)	7.88 (6.5 - 8.5)
St. dev	0.173	0.529	1.396	7.633	0.340
Skewness	-0.243	0.332	-0.562	1.266	0.874
Kurtosis	-1.114	-0.936	-0.671	4.264	2.766
*Values in brackets represent the standard limits as defined by NSDWG					

Table 4.2. Correlation matrix of water quality parameters

<b>Variables</b>	<b>Phosphate (mg/L)</b>	<b>Nitrate (mg/L)</b>	<b>Turbidity (NTU)</b>	<b>EC (S/cm)</b>	<b>pH</b>
Phosphate (mg/L)	1				
Nitrate (mg/L)	0.684*	1			
Turbidity (NTU)	0.806*	0.713*	1		
EC (S/cm)	-0.005	-0.212	-0.194	1	
pH	0.235	0.168	0.108	0.472	1



## 4.2 ASD Spectral Signatures Processing

Figure 4.1 shows ASD spectra computed from in situ data collected on 11<sup>th</sup> July 2023. A few of the sample signatures show a small trough 400nm – 440 nm, this may suggest the presence of nitrates and phosphates as they both absorb light in blue and ultraviolet spectra. Also, the presence of algae or phytoplankton in blue spectrum absorbs light in this region. Secondly, turbidity is often associated with suspended particles in the water, such as organic matter, algae or sediments.

Higher turbidity levels influence reduced reflection in this spectrum due to increased scattering. Furthermore, all of the curves highlight the significant reflectance peak at the green region, i.e., 550- 600 nm, which is often associated with the red edge of chlorophyll absorption, as described by previous studies. Red edge is a point at which chlorophyll absorbs less strongly, leading to a peak in reflectance. This peak suggests the potential for algae or other photosynthetic organisms in water body. While nitrates and phosphates may not directly contribute to this peak, their presence can influence algae and phytoplankton growth, indirectly contributing to the observed chlorophyll related reflectance.

Similarly, the presence of turbidity impacts the absorption characteristics of water. In the 550 – 600nm range, chlorophyll absorption peaks are common, turbidity contribute to reducing absorption by scattering incident light away from particles with absorption features. This reduction in absorption, coupled with increased scattering, leads to a higher level of reflectance in the green spectrum. This trend can be observed in the sample 1 reflectance signature (top most signature in red color), it was taken near the edge of the dam where sediment concentrations were high due to this a small peak can also be observed in the NIR spectrum from 700 – 750 nm, also an overall increase of reflectance from other sample points. The downward trend toward the NIR region indicates an increase in absorption and reduced scattering in this region. Water typically exhibits higher NIR absorption absorption due to water molecules' strong bands.

### **4.3 Comparison Between Multispectral and Hyperspectral Data**

#### **4.3.1 Bands Selection**

To develop MLR models between Hyperspectral, Multispectral and Water quality parameters, different bands and wavelength ranges were selected, to get variable data, their ratios were extracted to reduce the noise and improve reflectance information. Table 4.3 details the selected bands of Landsat OLI and ASD wavelength ranges.

Correlation analysis between the reflectance ratios of various bands and turbidity and nutrient concentration of field data was used to identify the best bands and wavelengths for the approach for predicting the reflectance ratio in turbidity and nutrients concentration in Khanpur dam. For a correlation study, reflectance ratios between the 350–1000 nm wavelength range of ASD and bands 2–5 of Landsat were computed. The reflectance ratios 560/891nm, 600/820 nm and 465/729nm of ASD and Band3/Band5 and Band4/Band5 of OLI, had the highest correlation between turbidity and nutrient content, and were chosen for linear modelling based on the findings of the correlation study.

#### **4.3.2 Regression Model**

For regression analysis, linear polynomial model is used and for the dependent variable, the associated turbidity and nutrients (phosphates and nitrates) concentrations were considered, while the independent variables were the spectral reflectance wavelength ratios for ASD data and band ratios for multispectral data. Results and graphs of the predicted models are given below.

##### **4.3.2.1 Turbidity**

Turbidity concentration in Khanpur dam is estimated using ASD ratio 560/891nm and OLI ratio Band3/Band5 giving the value of  $r = 0.86$  and  $0.64$  respectively as describe in Figure: 4.2 (a) & (b). While ASD ratio 600/820nm and OLI ratio Band4/Band5 gives the value of  $r = 0.71$  and  $r = 0.84$  as explained in Figure: 4.2 (c) & (d).

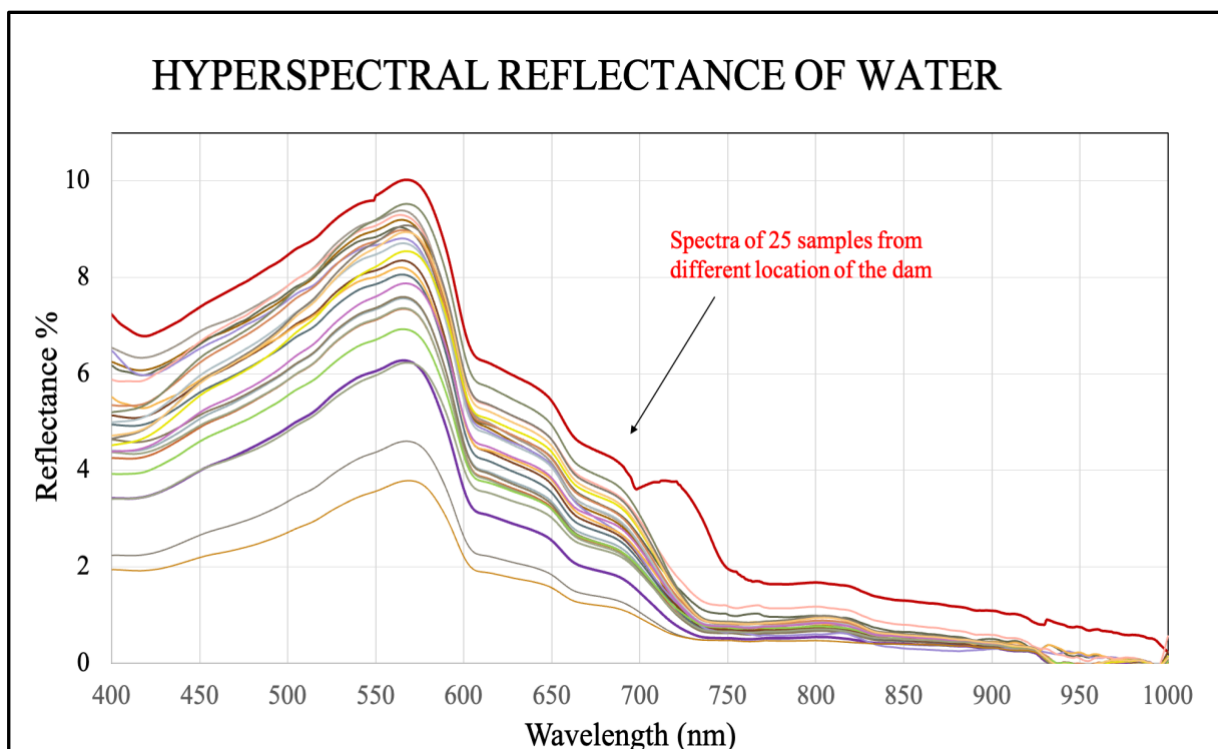


Figure 4.1. ASD-hyperspectral reflectance signatures from 25 different locations of Khanpur dam.

Table 4.3. Selected wavelengths and their ranges.

Landsat 8 OLI Bands & Their Ranges (nm)		ASD-Hyperspectral VNIR Spectrum Wavelength Ranges (nm)	
<b>Band 2</b>	Blue (450-510)	<b>Blue</b>	400-500
<b>Band 3</b>	Green (530-590)	<b>Green</b>	500-600
<b>Band 4</b>	Red (640-670)	<b>Red</b>	600-700
<b>Band 5</b>	NIR (850-880)	<b>NIR</b>	700-1000

In comparison to OLI ratio Band3/Band5 the ASD ratio 560/891nm showed a much better correlation coefficient, indicating a greater linear relationship between the turbidity concentration and the selected spectral ratio for the ASD spectroradiometer.

Similarly, the OLI ratio Band4/Band5 revealed a greater connection with turbidity than the ASD ratio 600/820nm, suggesting that the OLI sensor is effective in assessing turbidity based on this particular ratio. Overall, ASD ratio 560/891nm gives better linear fit model than OLI for turbidity.

#### 4.3.2.2 Phosphate

Figure 4.3 (a) predicts the linear model for phosphate with ASD ratio 560/891 and gives the value of  $r = 0.83$  whereas, Figure (b) describes the regression model for phosphate with OLI ratio of band3/band5 gives  $r = 0.72$ . In contrast, figure (c) shows the linear model which predicts phosphate concentration with ASD ratio 600/820nm and gives the value of  $r = 0.83$  and Figure (d) depicts the value of  $r = 0.70$  for phosphates with OLI band4/band5 ratio. Overall, it can be seen that both ratios of hyperspectral data give better results than multispectral data for phosphate estimation in Khanpur dam.

#### 4.3.2.3 Nitrate

For the prediction of nitrate concentration instead of the green spectrum, wavelength range of blue spectrum is being used as it was described in literature that nitrate ions respond strongly to blue wavelength range. So, Figure 4.4 (a) gives us the value of  $r = 0.86$  for linear model of nitrate and ASD ratio 465/729nm whereas Figure (b) gives us value of  $r = 0.67$  for model between nitrate and OLI band2/band5. On the contrary, regression model of nitrate with ASD ratio 600/820 nm gives  $r = 0.73$  and linear model of nitrate and OLI band4/band5 gives  $r = 0.76$  as shown in Figure (c) & (d). Particularly, ASD predicts best line fit model for nitrate concentration with ratio 465/729 nm.

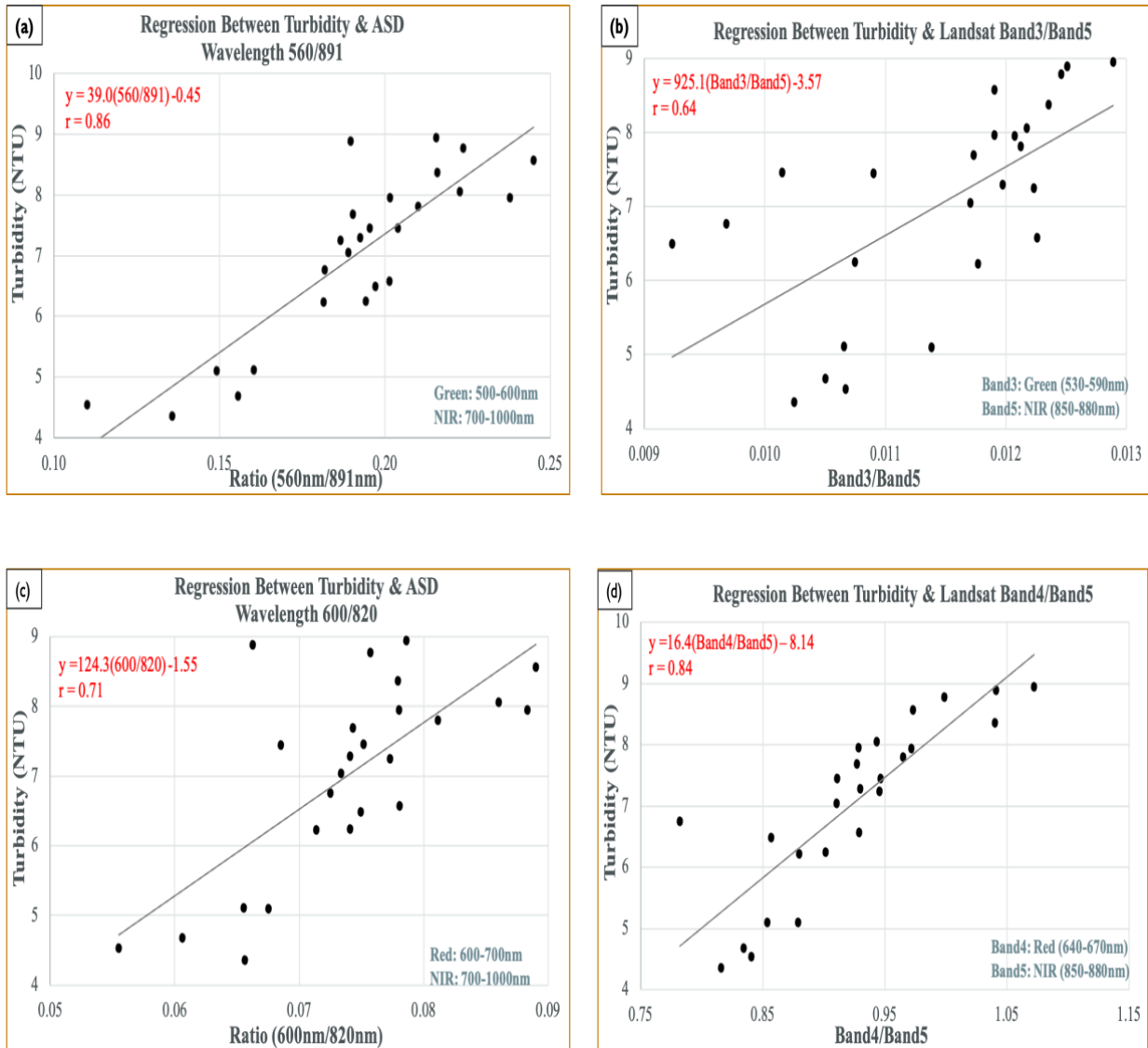


Figure 4.2 (a) Regression Model of Turbidity and Wavelength ratio 560/891nm ratio of ASD; (b) Regression Model of Turbidity and OLI\_Band3/Band4 ratio; (c) Regression Model of Turbidity and ASD Wavelength 600/820nm ratio; (d) Regression Model of Turbidity and OLI\_Band4/Band5

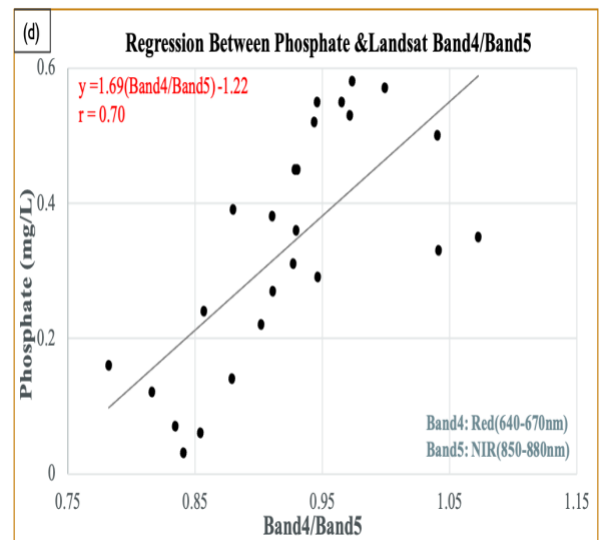
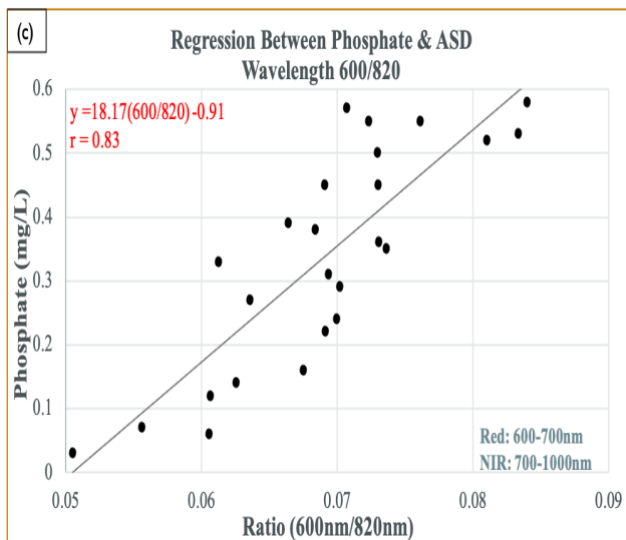
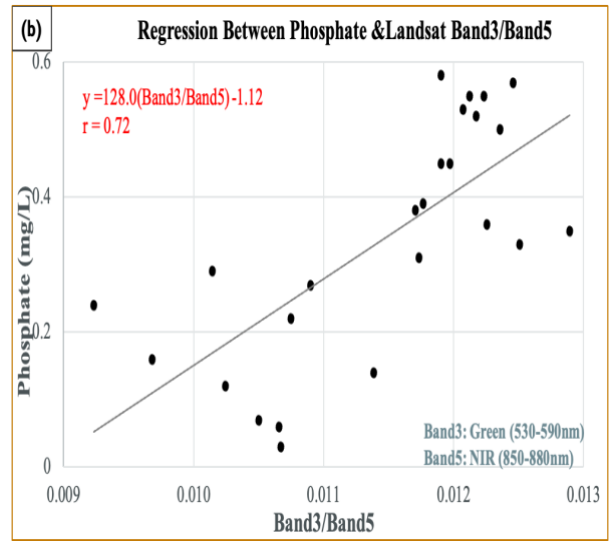
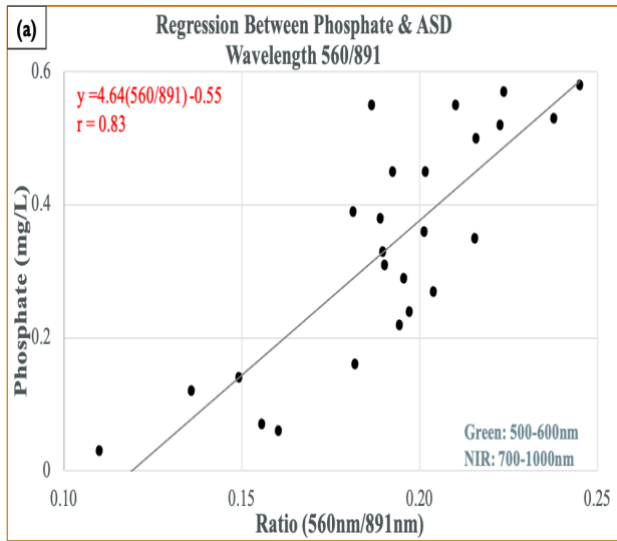


Figure 4.3 a) Regression Model of Phosphate and ASD Wavelength 560/891nm ratio; (b) Regression Model of Phosphate and OLI\_Band3/Band5 ratio; (c) Regression Model of Phosphate and ASD Wavelength 600/820nm ratio; (d) Regression Model of Phosphate and OLI\_Band4/Band5

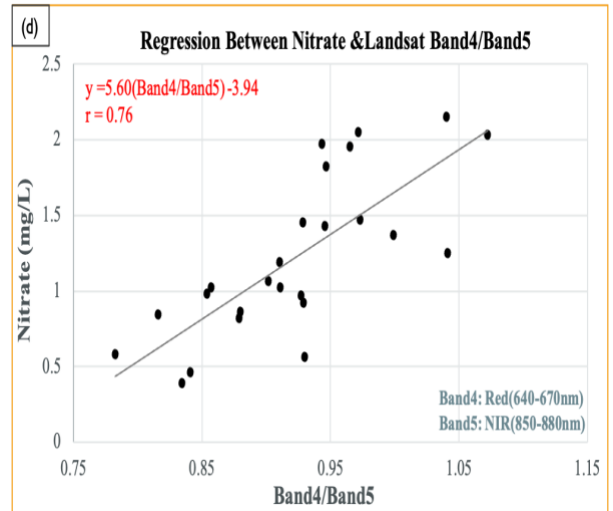
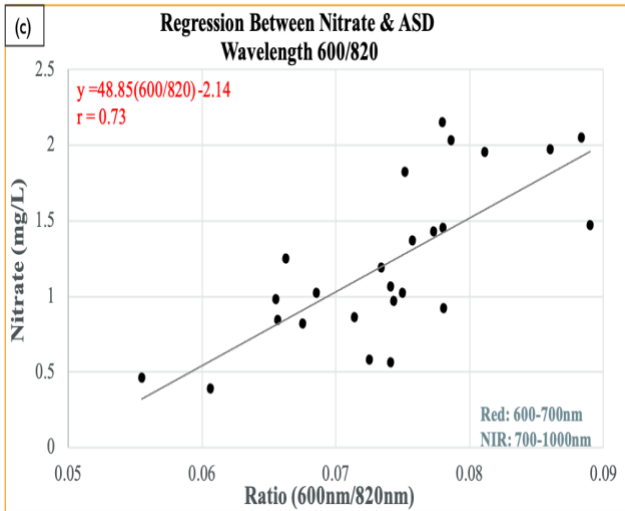
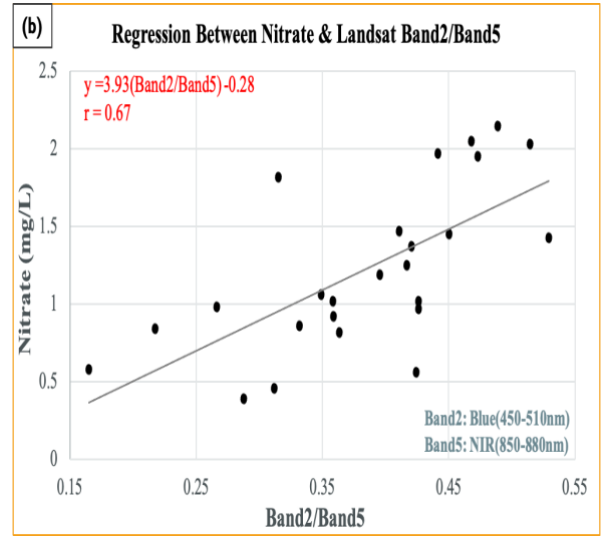
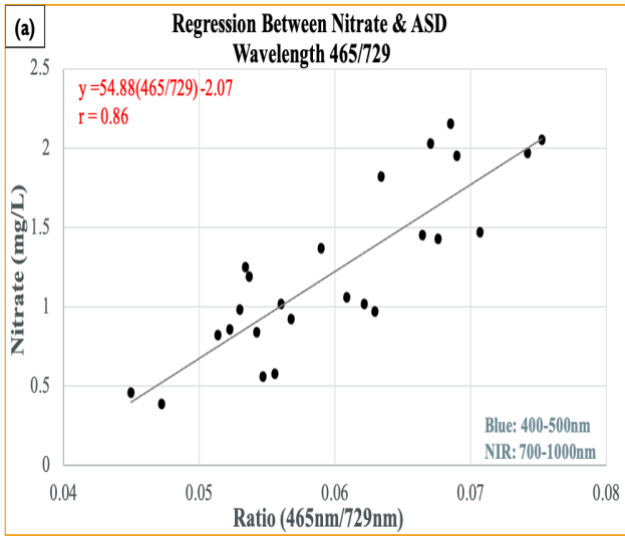


Figure 4.4 a) Regression Model of Nitrate and ASD Wavelength 465/729nm ratio; (b) Regression Model of Nitrate and OLI\_Band2/Band5 ratio; (c) Regression Model of Nitrate and ASD Wavelength 600/820nm ratio; (d) Regression Model of Nitrate and OLI\_Band4/Band5

## 4.4 Model Validation

Different matrices like  $r$ ,  $R^2$  and RMSE are used for linear model validation.

### 4.4.1 Turbidity

Table 4.4 shows the regression equation obtained from the linear model predicted for turbidity concentration and its validation parameters like root mean square error and determination of coefficient  $R^2$ , with selected ASD reflectance ratios. Table 4.5 shows the above-mentioned parameters with Landsat OLI-selected ratios. Among all the calibrations tested, the best fit model using ASD wavelengths was obtained from Ratio 560/891 nm with a value of  $R^2 = 0.75$  and RMSE 0.68. Comparably, among the models using OLI ratios, the best fit model was obtained using ratio Band4/Band5 having the value of  $R^2 = 0.71$  and RMSE 0.96. These results concluded that, although both of these ratios of ASD and OLI gave best fit models. But ASD model gave more accurate findings than OLI.

### 4.4.2 Phosphate

Table 4.6 shows the regression equation for phosphate concentration prediction that was obtained using the linear model via specific ASD reflectance ratios, along with validation metrics like root mean square error (RMSE) and the determination coefficient ( $R^2$ ). On the other hand, Table 4.7 uses Landsat OLI selected ratios to provide the previously suggested attributes. Among the various calibrations examined, the optimal model employing ASD wavelengths was identified based on Ratio 560/891 nm and 600/820 nm. These ratios demonstrated minimal disparity in prediction but yielded  $R^2$  values of 0.69 for both, accompanied by respective RMSE values of 0.10 and 0.09. On the other hand, the Band4/Band5 ratio was the best-fitting model among those that used OLI ratios; it had an  $R^2$  value of 0.49 and an RMSE of 0.09. In addition, an  $R^2$  value of 0.57 with an RMSE of 0.11 was obtained from the Band2/Band5 ratio. The ASD and OLI ratios produced well-fitting models, the ASD model demonstrated superior predictive accuracy for phosphate concentration.



Table 4.4. Model validation results of turbidity with ASD ratios.

<b>Ratios</b>	<b>Model</b>	<b>R<sup>2</sup></b>	<b>RMSE</b>
465/729	$y = 116.3(465/729) + 0.04$	0.47	0.99
560/891	$y = 39.0(560/891) - 0.45$	0.75	0.68
600/820	$y = 124.3(600/820) - 1.55$	0.50	0.96

Table 4.5. Model validation results of turbidity with OLI ratios.

<b>Ratios</b>	<b>Model</b>	<b>R<sup>2</sup></b>	<b>RMSE</b>
Band2/Band5 (450-510/850-880)	$y = 11.06(\text{Band2/Band4}) - 2.77$	0.51	0.96
Band3/Band5 (530-590/850-880)	$y = 925.1(\text{Band3/Band5}) - 3.57$	0.41	1.04
Band4/Band5 (640-670/850-880)	$y = 16.4(\text{Band4/Band5}) - 8.14$	0.71	0.73

Table 4.6. Model validation results of phosphate with ASD ratios.

<b>Ratios</b>	<b>Model</b>	<b>R<sup>2</sup></b>	<b>RMSE</b>
465/729	$y = 15.70(465/729) - 0.60$	0.56	0.11
560/891	$y = 4.64(560/891) - 0.55$	0.69	0.10
600/820	$y = 18.17(600/820) - 0.91$	0.69	0.09

Table 4.7. Model validation results of phosphate with OLI ratios.

<b>Ratios</b>	<b>Model</b>	<b>R<sup>2</sup></b>	<b>RMSE</b>
Band2/Band5 (450-510/850-880)	$y = 1.46(\text{Band2/Band4}) - 0.22$	0.57	0.11
Band3/Band5 (530-590/850-880)	$y = 128.0(\text{Band3/Band5}) - 1.12$	0.51	0.12
Band4/Band5 (640-670/850-880)	$y = 1.69(\text{Band4/Band5}) - 1.22$	0.49	0.09

### 4.4.3 Nitrate

To predict nitrate concentration given particular ASD reflectance ratios, a linear model yielded the regression equation shown in Table 4.4.3(a). This table also includes validation measures to evaluate the model's accuracy, such as the determination coefficient ( $R^2$ ) and the root mean square error (RMSE). On the other hand, Table 4.4.3(b) presents the previously described regression model equation and validation metrics using Landsat OLI chosen ratios, providing a different viewpoint on the model's prediction ability. Using ASD wavelengths, the Ratio 465/729 nm was the best model among the calibrations. This led to a low root mean square error (RMSE = 0.27) and a significant correlation ( $R^2 = 0.74$ ) for the prediction of nitrate levels. In contrast, with an  $R^2$  value of 0.58 and an RMSE of 0.96, the Band4/Band5 ratio was found to be the most appropriate model when employing Landsat OLI ratios. These findings indicate that in terms of accuracy in forecasting nitrate concentration, the ASD-derived model that is, the model based on Ratio 465/729 nm performs better than the OLI-based model. Higher  $R^2$  and lower RMSE values highlight the ASD model's better prediction ability in this investigation by pointing to a stronger association between the target variable and particular spectral ratios.

For all three water quality parameters, ASD ratios consistently surpassed Landsat ratios over a wide range of wavelengths. The superiority of ASD ratios over a wide range of wavelengths highlights their adaptability and extensive spectrum coverage, making it possible to derive precise models for various water quality indicators. Because of its competency in the Band4/Band5 area, Landsat is useful for some metrics, but its application to a larger variety of water quality indicators may be limited due to its absence of the wider spectrum coverage offered by ASD. The precise water quality metrics under consideration and the spectral features that best capture their fluctuation will determine whether ASD and Landsat ratio are the best options.

Table 4.8. Model validation results of nitrate with ASD ratios.

<b>Ratios</b>	<b>Model</b>	<b>R<sup>2</sup></b>	<b>RMSE</b>
465/729	$y = 54.88(465/729) - 2.07$	0.74	0.27
560/891	$y = 12.15(560/891) - 1.10$	0.50	0.36
600/820	$y = 48.85(600/820) - 2.14$	0.54	0.35

Table 4.9. Model validation results of nitrate with OLI ratios.

<b>Ratios</b>	<b>Model</b>	<b>R<sup>2</sup></b>	<b>RMSE</b>
Band2/Band5 (450-510/850-880)	$y = 3.93(\text{Band2/Band5}) - 0.28$	0.45	0.38
Band3/Band5 (530-590/850-880)	$y = 282.1(\text{Band3/Band5}) - 2.00$	0.26	0.44
Band4/Band5 (640-670/850-880)	$y = 5.60(\text{Band4/Band5}) - 3.94$	0.58	0.34

## 4.5 Water Quality Indices

Remote sensing water quality indices taken from (Mazhar et al., 2023) were applied on Landsat 8 image to visually represent the overall quality of Khanpur dam.

### 4.5.1 Normalized Difference Chlorophyll Index (NDCI)

Eutrophication is the main indicator of water quality, as chlorophyll-a is present in all types of phytoplankton thus NDCI helps to map chlorophyll content present in water.

Formula:

$$\text{NDCI} = \text{NIR}/\text{GREEN}-1$$

Figure 4.5 shows that high value of 0.72 in NDCI represents presence of vegetation as this value is closer to 1. Meanwhile, the low value of -0.24 represents clear water as this value is closer to -1. From this map it is clear that if any of the eutrophication or algal blooms are present in the water body, they are present on the edges of the dam. This is because eutrophication concentrates at the dam edges due to shallower waters, limited circulation, and increased exposure to runoff, promoting sediment resuspension and nutrient accumulation in these areas. Moreover, NDCI is applied on the image to detect chlorophyll concentration. This approach and due to the absence of established indices in existing literature that are capable of directly quantifying nutrient levels, such as nitrates and phosphates, within water bodies. These nutrients are known to foster the proliferation of algal blooms. The utilization of NDCI serves as a robust method for indirectly gauging the nutrient content in water, providing valuable insights into potential algal bloom development.

### 4.5.2 Normalized Difference Turbidity Index (NDTI)

NDTI is used to detect turbid water with the help of remotely sensed images. Negative values indicate clear water, whereas positive values indicate turbid water.

Formula:

$$\text{NDTI} = \text{Red}-\text{Green}/\text{Red}+\text{Green}$$

In Figure 4.6 the values closer to the negative range represent clear water, thus, the high value of 0.03 in NDTI map output is closer to zero and the low value of -0.08 indicates very low amounts of turbidity that is present in the water body. Similarly, as in NDCI, turbidity is observed predominantly along the peripheries of the dam, attributed to the shallowness of the water in these zones, resulting in heightened reflection of the underlying soil surface. Additionally, the accumulation of runoff from upstream contributes to increased turbidity levels in these specific areas. Notably, the influx and outflow of water within the dam mitigate this accumulated turbidity by facilitating the removal of sediments and suspended particles, thereby influencing the overall water clarity in the reservoir.

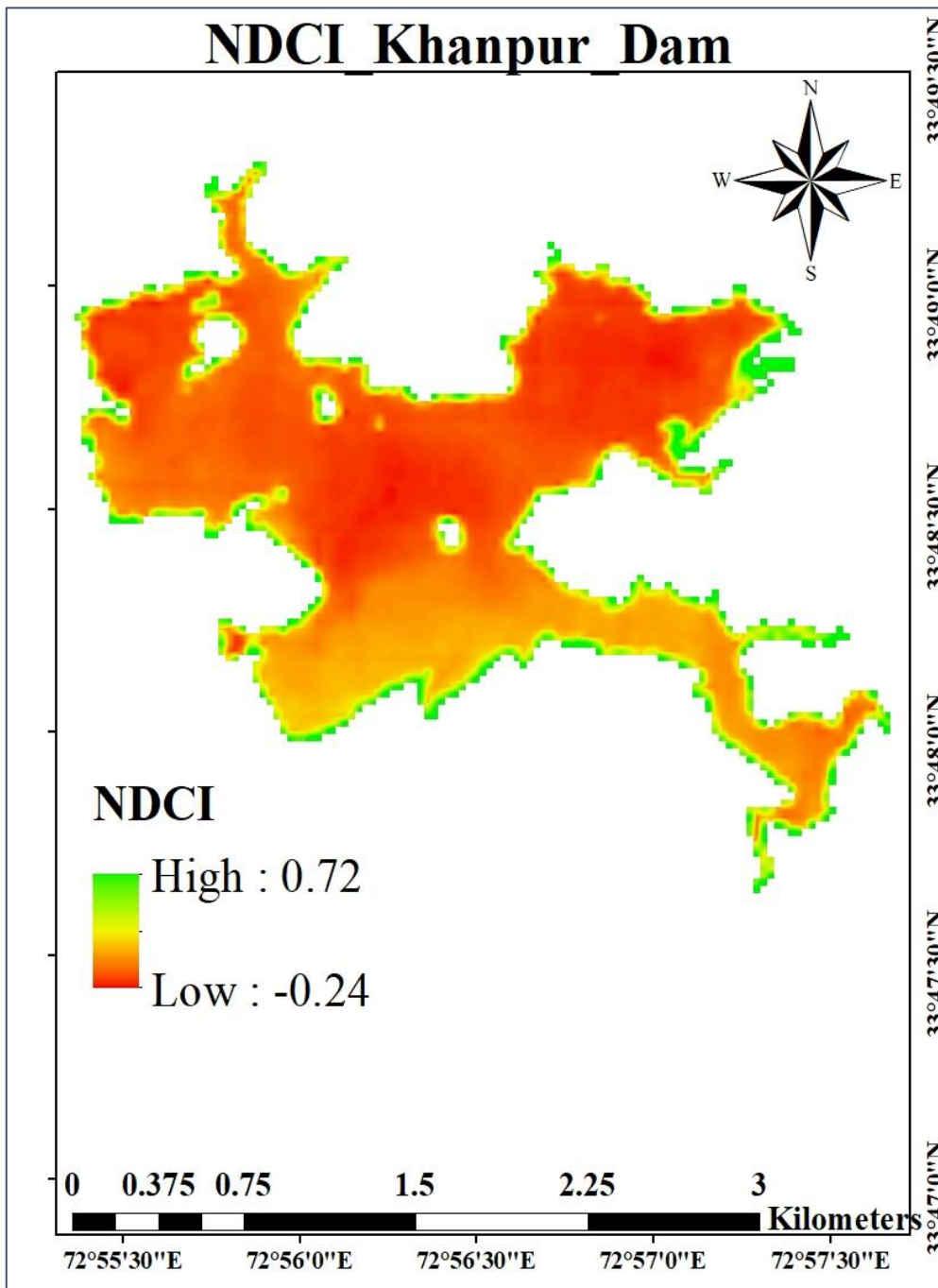


Figure 4.5. Normalized difference chlorophyll index map of Khanpur Dam.

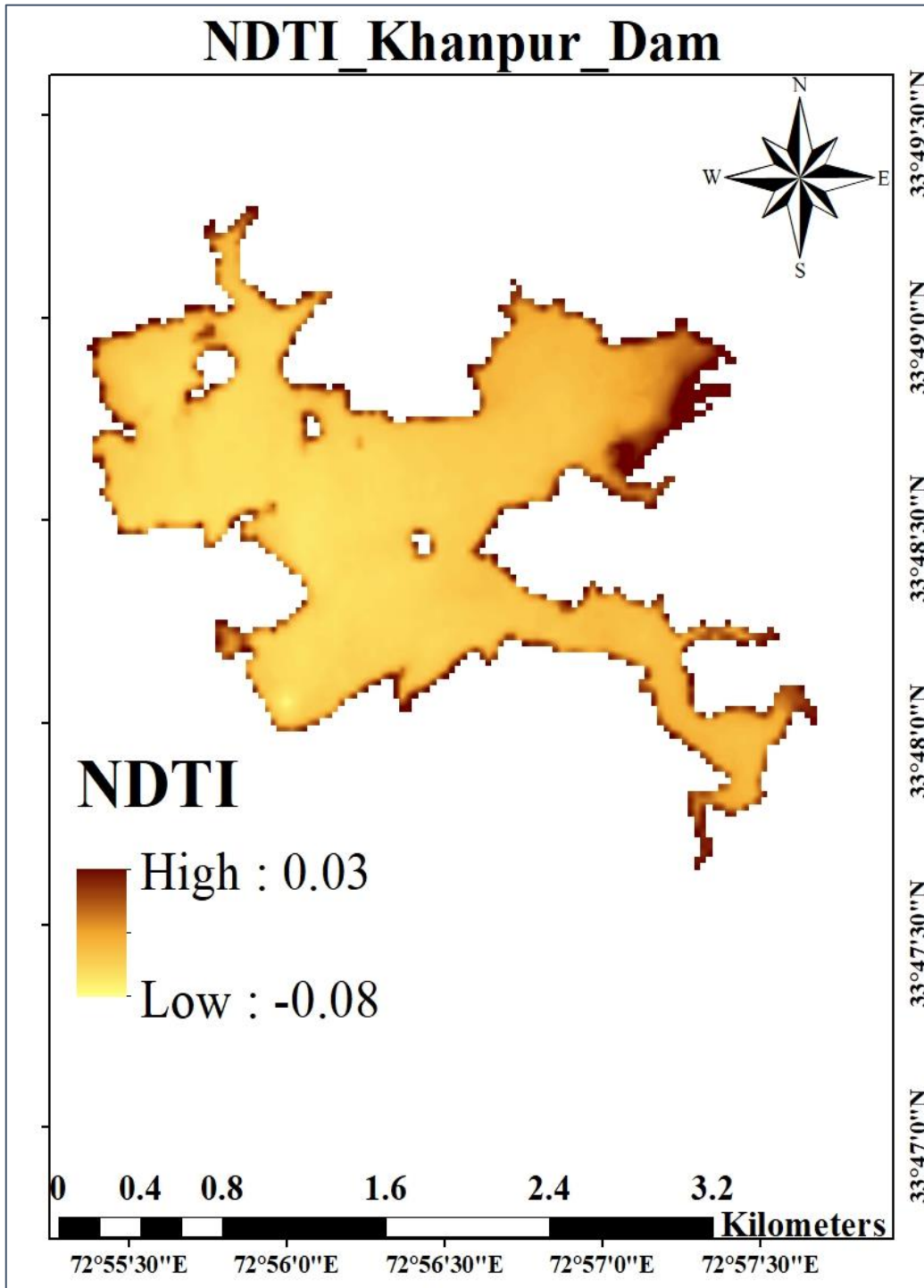


Figure 4.6. Normalized difference turbidity index map of Khanpur Dam.



### CONCLUSIONS AND RECOMMENDATIONS

#### 5.1 Conclusions

The findings derived from laboratory analysis of water quality parameters indicate that the water quality of Khanpur dam is deemed satisfactory. pH, EC and nitrates are within the permitted threshold set by NSDWG. While concentrations of phosphates and turbidity surpass the permissible limits, their magnitudes are exceedingly minute, rendering them negligible in practical terms.

By comparing the regression model results, it was concluded that band ratios that correlate with the ground data vary from one study area to another. The analysis of selected wavelength ratios from ASD-hyperspectral data revealed noteworthy correlations. Specifically, the ratio 560/891 demonstrated a correlation coefficient ( $r$ ) of  $\geq 0.8$  for both turbidity and phosphates. Meanwhile, the ratio 600/820 exhibited a correlation coefficient of  $r = 0.7$  across all three parameters. Meanwhile, the ratio 465/729 yielded a substantial correlation ( $r = 0.86$ ) for the nitrate parameter. Meanwhile, from OLI/Landsat 8 data, the red/NIR ratio yielded a robust correlation ( $r \geq 0.7$ ) for nitrates, phosphates, and turbidity, while the blue/NIR and green/NIR ratios achieved a correlation coefficient of  $r = 0.6$ . These findings underscore the effectiveness of specific wavelength ratios in capturing distinct water quality parameters, with the OLI/Landsat 8 red/NIR ratio demonstrating notable consistency across multiple parameters. Although satisfactory fits were obtained, validation of the models showed that fitted models of ASD ratios achieved more accurate results than OLI bands using RMSE, as ASD collects spectra in a narrower wavelength range, thus allowing more targeted and precise analysis of parameters and helps discern subtle variations in the water quality. Turbidity achieved best-fit model with a ratio 560/891nm having RMSE of 0.68 and  $R^2 = 0.75$  for ASD data. In comparison, the OLI ratio of Band3/Band5 gives RMSE of 1.04 and  $R^2 = 0.41$ . For

phosphates, ASD ratio 600/820 nm having RMSE of 0.09 and  $R^2 = 0.69$  achieved better-suited model than OLI ratio Band4/band5 whose RMSE is 0.09 but  $R^2$  is 0.49. Similarly, for nitrates, ASD ratio 465/729 nm achieved  $R^2 = 0.74$  and RMSE of 0.27, whereas OLI ratio Band2/Band5 gave  $R^2 = 0.45$  and RMSE of 0.38.

Utilizing Landsat indices and ASD reflectance spectra, the investigation determined that the dam predominantly exhibits clear water. As shown in NDCI and NDTI maps representing water body having predominantly negative values, attribute with low turbidity and chlorophyll concentration. When identified, instances of turbidity or eutrophication are localized at the edges of the dam, and their dissipation is facilitated through the natural inflow and outflow of water.

## **5.2 Recommendations**

1. The dam's Water quality parameters must be checked regularly using remote sensing and laboratory analysis.
2. Traditional water sampling analysis methods are expensive and time-consuming, so there is a need of inexpensive and accurate methods. This is where the remote sensing methods come in handy for site-specific management and water quality variability mapping.
3. Once a robust remote sensing model is developed, it should be utilized in future water quality monitoring.
4. There is a compelling need to explore commercially available remote sensing data characterized by high spectral and spatial resolution than Landsat OLI, as such data may potentially enhance the development of more effective models. This exploration aligns to continually advance the precision and reliability of water quality assessment methodologies.

5. Climate change may influence the quality of water and adaptation measures to climate change must be taken into account in water management plans based on this precise modeling. This is particularly crucial in areas where precipitation patterns may fluctuate, like Pakistan.
6. The study's findings provide important new information to policymakers by emphasizing the need to plan how to create policies that prioritize long-term sustainable urban development planning in the upstream urban centers and regulate anthropogenic activities that impact the reservoir's water quality. With the help of these policy actions, the reservoir's ability to retain water will be improved, guaranteeing its continuous use for the benefit of future generations.

## REFERENCES

1. A. Pisanti, S. Magri, Ferrando, I. and Federici, B. (2022). Sea water turbidity analysis from sentinel-2 images: atmospheric correction and bands correlation. *The International Archives of the Photogrammetry, Remote Sensing and Spatial Information Sciences*, XLVIII-4/W1-2022, pp.371–378. doi:<https://doi.org/10.5194/isprs-archives-xxviii-4-w1-2022-371-2022>.
2. Ahmed, M., Mumtaz, R. and Hassan Zaidi, S.M. (2021). Analysis of water quality indices and machine learning techniques for rating water pollution: a case study of Rawal Dam, Pakistan. *Water Supply*. doi:<https://doi.org/10.2166/ws.2021.082>.
3. Akbar, S., Nazir, A. and Shah, S.A. (2022). Analysis of Physico-Chemical and Microbiological Parameters of Rawal and Khanpur Dams. *International Journal of Scientific Research in Chemical Sciences*, [online] 9(2), pp.01–07. Available at: [www.isroset.org](http://www.isroset.org) [Accessed 20 Feb. 2022].
4. Bevans, R. (2020). *Understanding P values / Definition and Examples*. [online] Scribbr. Available at: <https://www.scribbr.com/statistics/p-value/#:~:text=The%20p%20value%20is%20a>.
5. Brezonik, P., Menken, K.D. and Bauer, M. (2005). Landsat-based Remote Sensing of Lake Water Quality Characteristics, Including Chlorophyll and Colored Dissolved Organic Matter (CDOM). *Lake and Reservoir Management*, 21(4), pp.373–382. doi:<https://doi.org/10.1080/07438140509354442>.
6. Calijuri, M.C. (2002). Temporal changes in the phytoplankton community structure in a tropical and eutrophic reservoir (Barra Bonita, S.P.--Brazil). *Journal of Plankton Research*, 24(7), pp.617–634. doi:<https://doi.org/10.1093/plankt/24.7.617>.
7. Dall’Olmo, G. and Gitelson, A.A. (2006). Effect of bio-optical parameter variability and uncertainties in reflectance measurements on the remote estimation of chlorophyll-a concentration in turbid productive waters: modeling results. *Applied Optics*, 45(15), p.3577. doi:<https://doi.org/10.1364/ao.45.003577>.
8. Dębska, K., Rutkowska, B. and Szulc, W. (2021). The influence of a dam reservoir on water quality in a small lowland river. *Environmental Monitoring and Assessment*, 193(3). doi:<https://doi.org/10.1007/s10661-021-08905-6>.
9. Duan, W., He, B., Takara, K., Luo, P., Nover, D., Sahu, N. and Yamashiki, Y. (2013a). Spatiotemporal evaluation of water quality incidents in Japan between 1996 and 2007. *Chemosphere*, 93(6), pp.946–953. doi:<https://doi.org/10.1016/j.chemosphere.2013.05.060>.
10. Duan, W., Takara, K., He, B., Luo, P., Nover, D. and Yamashiki, Y. (2013b). Spatial and temporal trends in estimates of nutrient and suspended sediment loads in the Ishikari River, Japan, 1985 to 2010. *Science of The Total Environment*, 461-462, pp.499–508. doi:<https://doi.org/10.1016/j.scitotenv.2013.05.022>.

11. Elhag, M., Gitas, I., Othman, A., Bahrawi, J. and Gikas, P. (2019). Assessment of Water Quality Parameters Using Temporal Remote Sensing Spectral Reflectance in Arid Environments, Saudi Arabia. *Water*, 11(3), p.556. doi:<https://doi.org/10.3390/w11030556>.
12. Faizi, F. and Mahmood, K. (2022). Synergic use of neural networks model and remote sensing algorithms to estimate water clarity indicators in Khanpur reservoir, Pakistan. *Acta Geophysica*, 70(3), pp.1433–1443. doi:<https://doi.org/10.1007/s11600-022-00790-y>.
13. Garg, V., Senthil Kumar, A., Aggarwal, S.P., Kumar, V., Dhote, P.R., Thakur, P.K., Nikam, B.R., Sambare, R.S., Siddiqui, A., Muduli, P.R. and Rastogi, G. (2017). Spectral similarity approach for mapping turbidity of an inland waterbody. *Journal of Hydrology*, [online] 550, pp.527–537. doi:<https://doi.org/10.1016/j.jhydrol.2017.05.039>.
14. Gholizadeh, M., Melesse, A. and Reddi, L. (2016). A Comprehensive Review on Water Quality Parameters Estimation Using Remote Sensing Techniques. *Sensors*, [online] 16(8), p.1298. doi:<https://doi.org/10.3390/s16081298>.
15. Górski, J., Dragon, K. and Kaczmarek, P.M.J. (2017). Nitrate pollution in the Warta River (Poland) between 1958 and 2016: trends and causes. *Environmental Science and Pollution Research*, 26(3), pp.2038–2046. doi:<https://doi.org/10.1007/s11356-017-9798-3>.
16. Goyens, C., Lavigne, H., Dille, A. and Vervaeren, H. (2022). Using Hyperspectral Remote Sensing to Monitor Water Quality in Drinking Water Reservoirs. *Remote Sensing*, 14(21), p.5607. doi:<https://doi.org/10.3390/rs14215607>.
17. Hafeez, S., Sing Wong, M., Abbas, S., Y. T. Kwok, C., Nichol, J., Ho Lee, K., Tang, D. and Pun, L. (2019). Detection and Monitoring of Marine Pollution Using Remote Sensing Technologies. *Monitoring of Marine Pollution*. [online] doi:<https://doi.org/10.5772/intechopen.81657>.
18. Harrison, J.A., Bouwman, A.F., Mayorga, E. and Seitzinger, S. (2010). Magnitudes and sources of dissolved inorganic phosphorus inputs to surface fresh waters and the coastal zone: A new global model. *Global Biogeochemical Cycles*, 24(1), p.n/a-n/a. doi:<https://doi.org/10.1029/2009gb003590>.
19. Harvey, E.T., Kratzer, S. and Philipson, P. (2015). Satellite-based water quality monitoring for improved spatial and temporal retrieval of chlorophyll-a in coastal waters. *Remote Sensing of Environment*, 158, pp.417–430. doi:<https://doi.org/10.1016/j.rse.2014.11.017>.
20. Hestir, E.L., Brando, V.E., Bresciani, M., Giardino, C., Erica Matta, E., Villa, P. and Dekker, A.G. (2015). Measuring freshwater aquatic ecosystems: The need for a hyperspectral global mapping satellite mission. *Remote Sensing of Environment*, [online] 167, pp.181–195. doi:<https://doi.org/10.1016/j.rse.2015.05.023>.
21. Huang, Y., Jiang, D., Zhuang, D. and Fu, J. (2010). Evaluation of Hyperspectral Indices for Chlorophyll-a Concentration Estimation in Tangxun Lake (Wuhan,

- China). *International Journal of Environmental Research and Public Health*, 7(6), pp.2437–2451. doi:<https://doi.org/10.3390/ijerph7062437>.
22. Iqbal, J. and Shah, M.H. (2014). Occurrence, risk assessment, and source apportionment of heavy metals in surface sediments from Khanpur Lake, Pakistan. *Journal of Analytical Science and Technology*, 5(1). doi:<https://doi.org/10.1186/s40543-014-0028-z>.
  23. Jadoon, W.A., Arshad, M. and Ullah, I. (2012). Spatio-temporal microbial water quality assessment of selected natural streams of Islamabad, Pakistan. *Records: Zoological Survey of Pakistan*, 21, pp.14–18.
  24. Kasuya, E. (2018). On the use of r and r squared in correlation and regression. *Ecological Research*, 34(1), pp.235–236. doi:<https://doi.org/10.1111/1440-1703.1011>.
  25. Kenton, W. (2022). *How Multiple Linear Regression Works*. [online] Investopedia. Available at: <https://www.investopedia.com/terms/m/mlr.asp#:~:text=Key%20Takeaways->.
  26. Khan, S.A., Khan, M., Khan, S.A. and Hussain, A. (2018). Determination of Physicochemical and Heavy Metals Concentration in Khanpur Dam Reservoir Khyber Pakhtunkhwa, Pakistan. *13th International Conference on Trends in Agricultural, Chemical, Environmental and Biological Sciences*. doi:<https://doi.org/10.17758/heaig4.h0618202>.
  27. Koronkevich, N., Barabanova, E., Georgiadi, A., Dolgov, S., Zaitseva, I. and Kashutina, E.A. (2019). Assessing the Anthropogenic Impact on the Water Resources of Russia. *Herald of the Russian Academy of Sciences*, [online] 89(3), pp.287–297. doi:<https://doi.org/10.1134/S1019331619030067>.
  28. Lin, Z., Huili, G., Wenji, Z., Xiaojuan, L., Jing, Z., Feina, L., Bo, Z. and Yanfang, X. (2009). Spectral features analysis of water quality in Baiyangdian wetland, China. *2009 17th International Conference on Geoinformatics*. doi:<https://doi.org/10.1109/geoinformatics.2009.5293240>.
  29. Mazhar, N., Javid, K., Akram, M.A.N., Afzal, A., Hamayon, K. and Ahmad, A. (2023). Index-Based Spatiotemporal Assesment Of Water Quality In Tarbela Reservoir, Pakistan (1990–2020). *GEOGRAPHY, ENVIRONMENT, SUSTAINABILITY*, 15(4), pp.232–242. doi:<https://doi.org/10.24057/2071-9388-2022-077>.
  30. Mir, A. (2022). *Khanpur Dam faces looming crisis of contamination*. [online] *The Express Tribune*. The Express Tribune. Available at: <https://tribune.com.pk/story/2376917/khanpur-dam-faces-looming-crisis-of-contamination>.
  31. Mishra, S. and Mishra, D.R. (2012). Normalized difference chlorophyll index: A novel model for remote estimation of chlorophyll-a concentration in turbid productive waters. *Remote Sensing of Environment*, 117, pp.394–406. doi:<https://doi.org/10.1016/j.rse.2011.10.016>.

32. MOORE, G.K. (1980). Satellite remote sensing of water turbidity / Sonde de télémessure par satellite de la turbidité de l'eau. *Hydrological Sciences Bulletin*, 25(4), pp.407–421. doi:<https://doi.org/10.1080/02626668009491950>.
33. Mortula, M., Ali, T., Bachir, A., Elaksher, A. and Abouleish, M. (2020). Towards Monitoring of Nutrient Pollution in Coastal Lake Using Remote Sensing and Regression Analysis. *Water*, 12(7), p.1954. doi:<https://doi.org/10.3390/w12071954>.
34. Muhammad Tayyab Sohail, Manzoor, Z., Ehsan, M., Nadhir Al-Ansari, Muhammad Bashir Khan, Shafi, A., Ullah, J., Hussain, A., Raza, D., Usman, U., Akbar, S. and Elbeltagi, A. (2023). Impacts of urbanization, LULC, LST, and NDVI changes on the static water table with possible solutions and water policy discussions: A case from Islamabad, Pakistan. *Frontiers in Environmental Science*, 11. doi:<https://doi.org/10.3389/fenvs.2023.1018500>.
35. Muhammad, S. and Ullah, I. (2022). Spatial and seasonal variation of water quality indices in Gomal Zam Dam and its tributaries of south Waziristan District, Pakistan. *Environmental Science and Pollution Research*, 29(19), pp.29141–29151. doi:<https://doi.org/10.1007/s11356-022-18524-4>.
36. Murugan, P., Sivakumar, R., Pandiyan, R. and Annadurai, M. (2016). Comparison of in-Situ Hyperspectral and Landsat ETM+ Data for Chlorophyll-a Mapping in Case-II Water (Krishnarajapuram Lake, Bangalore). *Journal of the Indian Society of Remote Sensing*, 44(6), pp.949–957. doi:<https://doi.org/10.1007/s12524-015-0531-8>.
37. Nauman, S., Zulkafli, Z., Bin Ghazali, A.H. and Yusuf, B. (2019). Impact Assessment of Future Climate Change on Streamflows Upstream of Khanpur Dam, Pakistan using Soil and Water Assessment Tool. *Water*, 11(5), p.1090. doi:<https://doi.org/10.3390/w11051090>.
38. Pakistan, A. (2017). *Khanpur Dam Ariel Photograph*. [Online] Available at: [https://twitter.com/amazing\\_pk/status/947384075156885504](https://twitter.com/amazing_pk/status/947384075156885504).
39. Petkovšek, G. (2017). Long-term modelling of reservoir sedimentation with turbid underflows. *Journal of Soils and Sediments*, 18(10), pp.3153–3165. doi:<https://doi.org/10.1007/s11368-017-1814-1>.
40. Rutherford, I.D., Kenyon, C., Thoms, M., Grove, J., Turnbull, J., Davies, P. and Lawrence, S. (2020). Human impacts on suspended sediment and turbidity in the River Murray, South Eastern Australia: Multiple lines of evidence. *River Research and Applications*, 36(4), pp.522–541. doi:<https://doi.org/10.1002/rra.3566>.
41. Sa'id and Mahmud, A. (2013). Spectrophotometric determination of nitrate and phosphate levels in drinking water samples in the vicinity of irrigated farmlands of kura town, kano state - nigeria. *ChemSearch Journal*, [online] 4, pp.47–50. Available at: <https://api.semanticscholar.org/CorpusID:92776342>.

42. Saleem, M., Iqbal, J. and Shah, M.H. (2015). Assessment of water quality for drinking/irrigation purpose from Mangla dam, Pakistan. *Geochemistry: Exploration, Environment, Analysis*, 16(2), pp.137–145. doi:<https://doi.org/10.1144/geochem2014-336>.
43. Senay, G., Shafique, N.A., Autrey, B., Fulk, F. and Cormier, S. (2002). The selection of narrow wavebands for optimizing water quality monitoring on the Great Miami River, Ohio using hyperspectral remote sensor data. *J. Spat. Hydrol.*, 1, pp.1–22.
44. Seyhan, E. and Dekker, A. (1986). Application of remote sensing techniques for water quality monitoring. *Hydrobiological Bulletin*, 20(1-2), pp.41–50. doi:<https://doi.org/10.1007/bf02291149>.
45. Swanson, H. and Zurawell, R. (2006). *Steele Lake Water Quality Monitoring Report - Provincial Parks Lake Monitoring Program*. [online] *DOC Player*. Monitoring and Evaluation Branch Environmental Assurance Division Alberta Environment: Alberta Environment . Available at: <http://docplayer.net/167680111-Steele-lake-water-quality-monitoring-report.html>.
46. Tsai, F. and Philpot, W.D. (1996). Derivative analysis of hyperspectral data. *Remote Sensing of Environment*. doi:<https://doi.org/10.1117/12.262471>.
47. Tyagi, K., Rane, C., Harshvardhan and Manry, M.T. (2022). Regression analysis. *Elsevier eBooks*, pp.53–63. doi:<https://doi.org/10.1016/b978-0-12-824054-0.00007-1>.
48. Watanabe, F., Alcântara, E., Rodrigues, T., Imai, N., Barbosa, C. and Rotta, L. (2015). Estimation of Chlorophyll-a Concentration and the Trophic State of the Barra Bonita Hydroelectric Reservoir Using OLI/Landsat-8 Images. *International Journal of Environmental Research and Public Health*, 12(9), pp.10391–10417. doi:<https://doi.org/10.3390/ijerph120910391>.
49. Wu, J.-L., Ho, C.-R., Huang, C.-C., Srivastav, A.L., Tzeng, J.-H. and Lin, Y.-T. (2014). Hyperspectral sensing for turbid water quality monitoring in freshwater rivers: Empirical relationship between reflectance and turbidity and total solids. *Sensors (Basel, Switzerland)*, [online] 14(12), pp.22670–22688. doi:<https://doi.org/10.3390/s141222670>.
50. Zhang, Y., Wu, L., Ren, H., Deng, L. and Zhang, P. (2020). Retrieval of Water Quality Parameters from Hyperspectral Images Using Hybrid Bayesian Probabilistic Neural Network. *Remote Sensing*, 12(10), p.1567. doi:<https://doi.org/10.3390/rs12101567>.